Guagliano *et al. Biochar* (2026) 8:39
https://doi.org/10.1007/s42773-025-00557-w

Biochar

ORIGINAL RESEARCH Open Access

Smart waste-derived materials for feed application: chestnut shells and vine pruning biochar

Marianna Guagliano[1*], Serena Reggi[2], Matteo Dell'Anno[2,3], Silvia Mostoni[4], Filippo Ottani[8], Marco Puglia[5], Giovanni Dotelli[1], Roberto Scotti[4,6], Simone Pedrazzi[5], Luciana Rossi[2], Cinzia Cristiani[1] and Elisabetta Finocchio[7]

Abstract

Carrier-assisted delivery is a key step for the successful targeted oral delivery of bioactive molecules in functional diets in livestock. The aim is to protect the biomolecule during gastric transit, and ensure its efficient release in the intestine. Biochar is the by-product of the thermochemical conversion of residual biomass in an oxygen-limited environment and has suitable physico-chemical and morphological properties to be a carrier. Two types of biochar were tested as carriers of egg white lysozyme (LY), selected as a representative of bioactive molecules both in terms of molecular size (MW 14.3 kDa) and antibacterial activity, for application in weaned pig feed. One biochar was derived from chestnut shells (CB) and the other from vine pruning (VB). An efficient and environmentally-friendly procedure for LY adsorption was developed, based on a solid/liquid process in mild conditions. The effects of the operating conditions, such as initial LY content, reaction time, and pH were also studied. The optimal conditions were found to be a maximum LY loading of 21–23 $mg_{LY}\ g_{Carrier}^{-1}$. Both pristine and hybrid materials were extensively characterized by combining morphological and physico-chemical techniques to obtain information on LY allocation and interactions with the carriers. Preliminary experiments on lysozyme release were performed at pH = 3 and pH = 7, simulating the pH conditions of the stomach and intestine of the weaned pigs, respectively. The results showed a higher releasing capacity when the pH was increased from 3 to 7. Specifically, the release showed a slight increase from 0.8% to 1.2% as the pH shifted from 3 to 7 for CB, and from 1.5% to 2.3% for VB. These results confirmed that biochar can protect LY from the low pH, during the gastric transit, and that LY could be released in the gut. These two benefits are likely related to the homogeneous distribution of LY molecules at the carrier surface, which is facilitated by the interaction of charges of opposite signs.

Highlights

- A simple methodology to adsorb lysozyme on biochar for feed application is proposed.
- The interaction between lysozyme and biochar is detailed.
- Higher lysozyme release at pH = 7 with our biochar-based carrier is observed.
- Targeted delivery in the intestinal environment is promoted by lysozyme release at pH = 7.

Keywords Biochar, Characterization, Animal feed, Lysozyme, Muramidase

*Correspondence:
Marianna Guagliano
marianna.guagliano@polimi.it
Full list of author information is available at the end of the article

Springer

Graphical Abstract

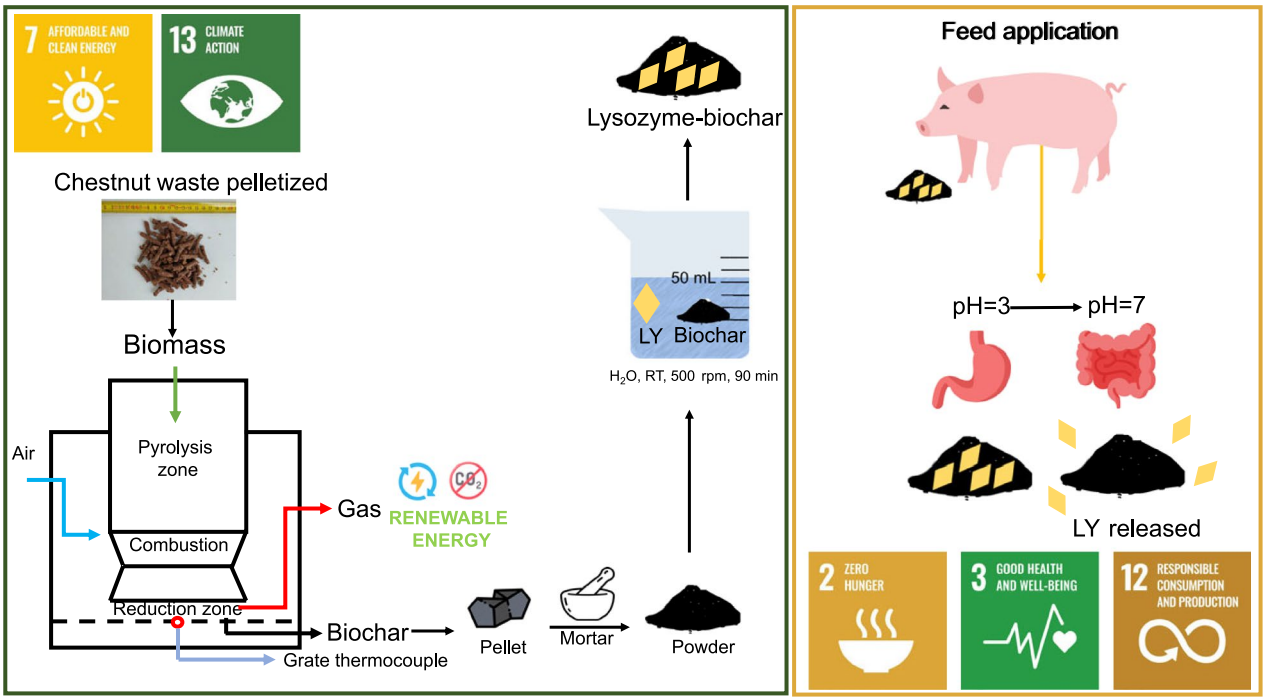

1 Introduction

Antimicrobial resistance (AMR) is a natural biological process that allows certain micro-organisms to survive or grow in the presence of an antibacterial agent and can be accelerated by the misuse and overuse of antibiotics (Prestinaci et al. 2015; Albernaz-Gonçalves et al. 2022).

AMR is a key threat to the future development of global public health (according to the World Health Organization, Centers for Disease Control and the European Centre for Disease Prevention and Control 2025). In addition to its significant impact on health-care systems, and beyond its direct implications for animal, human and environmental health, (Castañeda-Barba et al. 2024) AMR poses a significant challenge to economic progress. Combatting AMR entails using antibiotics only if strictly necessary and replacing them where possible (World Health Organization 2019).

In this regard, nutrition plays a pivotal role in host health, directly impacting gut health, which is strongly interconnected with the immune system and pathology development (Dell'Anno et al. 2023). Functional nutritional strategies represent a new frontier in diet formulation, supplementing bioactive compounds from various sources that positively influence both local gut and systemic health through multiple effects, such as antimicrobial, antioxidant, and anti-inflammatory activities (Kasapidou et al. 2015; Mahfuz et al. 2021). In the livestock system, significant steps have been taken to reduce the need for antimicrobials in food-producing animals, resulting in a substantial decrease in antibiotic use in Europe (Robinson et al. 2017; World Health Organization 2019) and around the world (Hu and Cowling 2020; Leistikow et al. 2022). However, the sustainability of the livestock sector should still be addressed through a holistic approach, including precision nutrition to enhance animal health and welfare, thereby reducing the occurrence of pathologies (Ramirez et al. 2019).

The weaning period is a critical phase in swine farming, since animals are exposed to different stressors that increase the risk of developing multifactorial diseases (Rossi et al. 2023). These conditions significantly impair piglets' health, often leading veterinarians to resort to antibiotic treatments to mitigate their detrimental effects on young animals (Ortiz Sanjuán et al. 2024). In the field of alternatives to antibiotics, which includes various molecules or strategies that can reduce the use of antibiotics through different mechanisms, lysozyme (LY) emerges as a promising option. This is a glycosidase enzyme able to kill or stop Gram-positive bacteria growth, making it

an interesting feed additive alternative to antibiotics (Wu et al. 2019; Kummer et al. 2023).

In fact, LY cleaves the glycosidic bond between N-acetylmuramic acid and N- acetylglucosamine residues of peptidoglycan, and lyses the Gram-positive bacteria barrier, thus hampering infection (Masschalck et al. 2001; Cromwell 2002; Ibrahim et al. 2002; Wu et al. 2019). LY is also known for its antiviral, antitumoral, and immune modulatory activities (Oliver and Wells 2015; Zou et al. 2019). Due to the antimicrobial properties reported above, LY is used mainly in pharmaceutical and food production applications (Dragoni et al. 2011; Silvetti et al. 2017). Recently, it has been studied as an additive for livestock feed as an alternative to the administration of antibiotics thanks to its antimicrobial properties (Oliver and Wells 2015; Ferraboschi et al. 2021).

The advantages of using LY as a feed additive in swine farming have been reported by several studies where LY is added to the weaned pig's diet in a concentration of 100–120 mg/kg. (Oliver and Wells 2015; Zou et al. 2019; Ferraboschi et al. 2021). Using functional additives in pig nutrition could reduce the occurrence of pathologies, thereby decreasing the need for antibiotic treatments and contributing to animal health in line with One Health principles (Liu et al. 2018b; Dell'Anno et al. 2020). Given that pigs share characteristics with humans in terms of anatomy, physiology, intestine dimensions, and microbiota composition, the results of studies on pigs could be potentially translated to human medicine and nutrition (Lunney et al. 2021).

A key challenge when administering LY orally is to prevent gastric degradation due to the combined actions of low stomach pH and the effect of hydrolases. Biochar is one of the possible innovative protective carriers, and it is the by-product of the thermochemical conversion of residual biomass in an oxygen-limited environment.

Biomass pyrolysis involves the thermal breakdown of the organic matrix of biomass in an oxygen-free environment, producing non-condensable gases, bio-oil, and biochar. Slow pyrolysis, also known as carbonization, is used to produce biochar and requires long residence times (several hours) and temperatures ranging from 300 to 700 °C (Kan et al. 2016).

The gasification process not only generates gas, but also produces tars (liquid) and biochar (solid) through the reaction of biomass with gasification agents such as air, steam, or oxygen, inside a gasifier at temperatures from 500 to 1200 °C, as reported in the supplementary material (Section S1).

Biochar is mainly made up of carbon, as well as hydrogen, oxygen, ash, and trace amounts of nitrogen. Depending on the process used, biochar can be characterized by a large surface area (SA), a porous structure, surface functional groups, and a high mineral content (Cha et al. 2016; Kalus et al. 2019; Yu et al. 2022). Biochar can be applied in different fields (Sakhiya et al. 2020), such as agriculture and the removal of pollutants (Jeffery et al. 2011; Jones et al. 2016; Li et al. 2019; Guo et al. 2020).

The benefits of using biochar to improve animal health have been known for several decades, however it has only recently been proposed as a feed ingredient for animal diets (Schmidt et al. 2019). Biochar's adsorption capability may be a natural way of preventing the harmful or fatal effects of orally ingested toxins, pesticides, and herbicides, such as glyphosate, or bacteriological pathogens (Gerlach 2014; Safaei Khorram et al. 2016; Cederlund et al. 2017; Mandal et al. 2017; Schmidt et al. 2019).

Supplementing biochar in animal feed can increase feed intake and weight gain, thereby strengthening the immune system, improving meat quality, and reducing the veterinary costs (Chen et al. 2019; Schmidt et al. 2019). The strong adsorption capacity of biochar can also reduce the environmentally harmful loss of ammonia through volatilization or leaching of nitrate, thus potentially reducing greenhouse gas emissions, such as nitrous oxide and methane derived from animal dejection (Jeffery et al. 2011; Chu et al. 2013a, 2013b; Kammann et al. 2017; Liu et al. 2018a; Borchard et al. 2019; Sha et al. 2019).

Unlike direct biomass firing, the co-production of energy and biochar in these processes also enables carbon sequestration (Brown 2021), as reported in the supplementary material (Section S2).

Moreover, biomass gasification is potentially a greener alternative to conventional biomass disposal, thus resulting in significant environmental benefits. For example, in Italy, where our study was carried out, the residual biomass from peeling chestnuts produces about 5300 tonnes of shells per year which are usually burned to be applied as fuel in facilities (Squillaci et al. 2018). Vine pruning produces a large amount of biomass residues, and in Italy more than 700,000 hectares are covered by vineyards (Picchi et al. 2013), with dry biomass production ranging between 1.0 and 2.5 tons per hectare (Zambon et al. 2018).

The use of such biomass for energy production via gasification, and reuse of the biochar produced, could play an important role in both the green transition and environmental protection in accordance with Italian research programs (PNR) 2021-272 and Horizon Europe (www.mur.gov.it, www.research-and-innovation.ec.europa.eu). In particular, chestnut shell biochar (CB), produced at Bio Energy Efficiency Laboratory, BEELab (Università degli studi di Modena e Reggio Emilia, UNIMORE), has been demonstrated as a viable carrier for LY due to its antimicrobial and antioxidant properties in feed

application (Reggi et al. 2025). Moreover, a comparison with a commercial vine pruning biochar (VB) (Romagna Carbone, Bagnacavallo, Italy), available in larger amount and considered as a benchmark, was also made.

The aim of this study was thus to assess the potential of using biochar, produced under controlled conditions, as a carrier for the protection and delivery of lysozyme under different pH conditions (pH = 3 and pH = 7), simulating the pH conditions of the stomach and intestine of the weaned pigs, respectively. We developed a model to enable the progress of targeted delivery systems for bioactive compounds, with a specific focus on implementing nutritional applications.

The novelty of this study lies in the use of biochar as a potential carrier of bioactive molecules, administered as a functional additive in animal feed, which is a relatively unexplored application for biochar. Indeed, although biochar has been reported as a feed additive, it has not been systematically studied as an oral carrier for protein-like bioactive molecules, such as LY.

2 Experimental

2.1 Materials

Lysozyme—99.9% pure powder of commercial chicken egg-white lysozyme, (LY) (CAS RN 12650-88-3, supplied by Sigma Aldrich, St. Louis, MO, USA) was used. LY is a compact complex ellipsoid-like molecule with dimensions of 4.5 × 3.0 × 3.0 nm (Cegielska-Radziejewska et al. 2008) whose molecular weight (MW) is 14.4 kDa. Lysozyme has an isoelectric point (IP) of + 11.35, and it remains positively charged below the pKa, due to the presence of 17 positively charged (6 lysines and 11 arginines) and nine negatively charged residues (7 aspartates and 2 glutamates) (Cegielska-Radziejewska et al. 2008; Wu et al. 2019).

For the carrier production, two types of biochar (**B**) were used:

- Commercial vine pruning biochar **(VB)** purchased from Romagna Carbone (Bagnacavallo, Italy). The VB carrier was produced by slow pyrolysis of the vine pruning waste in a temperature range from 450° to 500 °C. The process applies a proprietary batch pyrolysis procedure; therefore, no other details are available.
- Chestnut shell biochar **(CB)** was produced through gasification at temperatures of 600-800 °C. Chestnut shells, procured from Az. Agr. Agriappennino di Sepe Marco (Cecciola, Reggio Emilia, Italy), were pelletized (Fig. 1a,b) and used as fuel in the "Femto Gasifier," a laboratory-scale fixed-bed downdraft gasifier (schematic in Fig. 1c).

These two types of biochar (CB and VB) were tested as potential feed ingredients for weaned pigs (Reggi et al. 2024, 2025). Both biochars contain bioactive compounds with antioxidant and antimicrobial properties, which can inhibit the growth of pathogenic bacteria, such as *E. coli* (F4 + and F8 +), while promoting the growth of beneficial probiotic strains, including *Lactiplantibacillus plantarum* and *Limosilactobacillus reuteri.*

Pure HNO_3, NaOH (both supplied by Aldrich, 98% pure), and demineralized water were also used.

2.2 Methods

2.2.1 Lysozyme-biochar hybrid material preparation

Vine pruning and chestnut shell biochar-supported lysozyme samples, LY-VB and LY-CB respectively, were prepared by a solid/liquid adsorption procedure (Fig. 2). The effects of the operating parameters, such as LY concentration, pH and reaction time, as well as the biochar

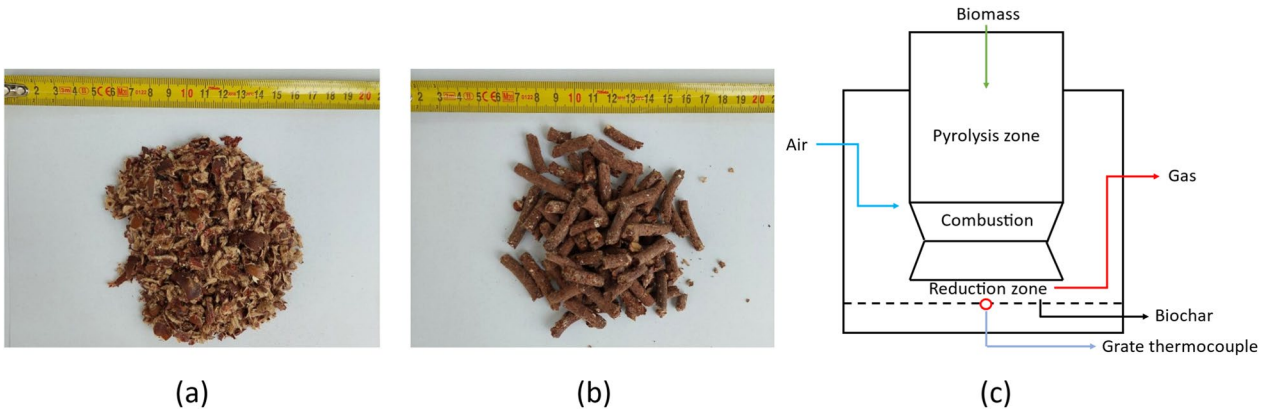

Fig. 1 **a** chestnuts shells, (**b**) pelletized chestnut shells, (**c**) schematic representation of the downdraft gasifier used for CB production

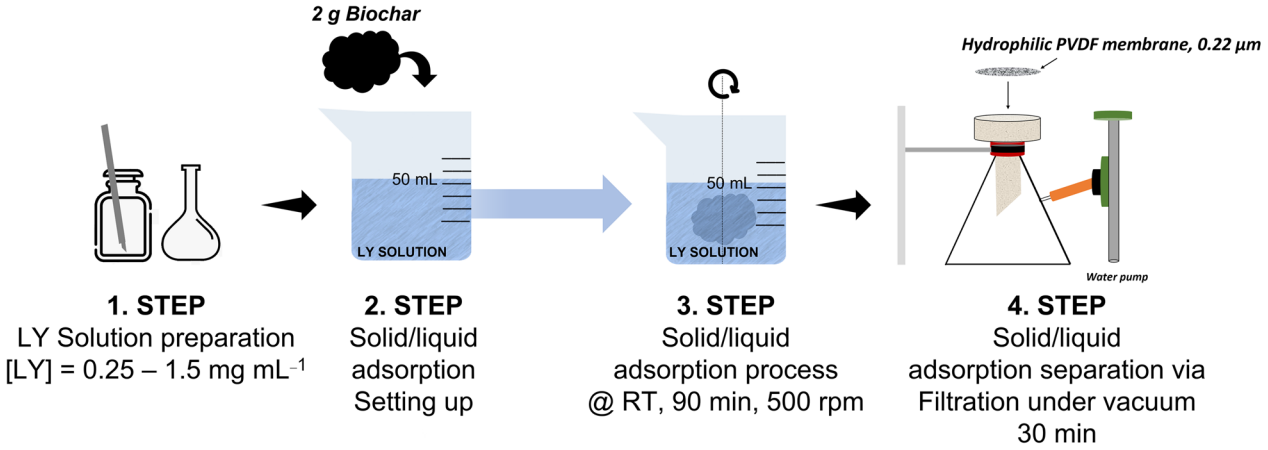

Fig. 2 Biochar-supported lysozyme preparation procedure

characteristics (nature and morphology) were considered. In a typical experiment, fixed amounts of LY (in the range 0.25–1.5 mg mL^{-1}) were dissolved in 50 mL of demineralized water, at room temperature (RT) under magnetic stirring (500 rpm); the dissolution took a few minutes. The initial constant solution pH in the range 4.5–4.7 was measured for all the LY concentrations. Subsequently, 2.0 g of bare biochar were added to the LY solution, and the obtained suspension was magnetically stirred at 500 rpm and RT for a fixed time (10–90 min). The pH of the suspension was monitored, but not corrected, throughout the experiment (glass electrode and pH-meter, Mettler Toledo Italia). Subsequently, the solids were separated by filtration under vacuum, using Durapore® polyvinylidene fluoride (PVDF) filter disks with a thickness of 125 µm and pore size of 0.22 µm which were purchased from Merck Millipore (Burlington, MA, USA).

No pH correction was performed during the contacting experiments, during which both types of biochar stabilized at pH = 8.8–9. In these pH conditions, LY is always reported as being positively charged (Cegielska-Radziejewska et al. 2008; Wu et al. 2019).

We also studied the mechanical mixture of biochar and LY, which was obtained by mixing pristine carriers and pristine LY as powder in a mortar, with 1 g of biochar mixed with 21 mg and 23 mg of LY. Thus, The LY-VB-MM and LY-CB-MM samples were prepared via simple mechanical mixing of their constituent components.

2.2.2 Liquid analysis

Chemical oxygen demand (COD) analysis was performed on the initial solutions and the liquids after uptake experiments. The measurement was conducted with a HANNA HI830 spectrophotometer in compliance with the EPA Method 410.4 (O'Dell 1996) and Standard Methods 5220 D.

The amount of captured LY was determined according to Eq. (1):

$$\begin{aligned} \mathrm{LY}capt\left(\mathrm{mg_{LY}/g_{Carrier}}\right) &= \mathrm{LY}ini\left(\mathrm{mg_{LY}/g_{Carrier}}\right) \\ &\quad -\mathrm{LY}res\left(\mathrm{mg_{LY}/g_{Carrier}}\right) \end{aligned} \quad (1)$$

where: "LY capt" is the amount of captured LY, "LY ini" is the amount of LY in the initial solution, and "LY res" is the residual LY in solution after the uptake reaction.

To check that there was no interference due to residues of the thermochemical conversion, selected samples of VB—i.e. the biochar obtained with the pyrolysis procedure at a temperature of 450–500 °C—were washed with demineralized water (50 mL) for durations between 10–300 min, at room temperature, while mixing at 500 rpm. After the suspension had been separated, the liquid was investigated via a COD analysis.

Negligible amounts of organic matter ranging from 0.02% to 0.05% (w/w) (Table S1), were released by the biochar, even after washing for 300 min. Accordingly, the following LY adsorption was performed without washing the biochar.

2.2.3 Characterization of solids

All the solids were analyzed by different physico-chemical analyses.

- Particle size was determined by Laser Granulometry (CILAS 1180) according to (Klank et al. 2009).
- Morphological analyses were performed by BET analysis (in N_2 atmosphere and bath temperature of 77.35 K), while the macroporosity was determined by Hg intrusion using an Autopore V9600 (Micromerit-

ics Instrument Corporation). The micropore volume and the external or non-microporous surface were analyzed by the t-method. Before the analysis, samples were degassed overnight at 120 °C, (heating rate from 25 °C to 60 °C, 1 °C min^{-1}).

- Elemental analysis (EA) was performed with Costech ECS mod.4010 which detects carbon, nitrogen, hydrogen, and sulfur.
- Zero point charge (ZPC) was determined by a Zetasizer Nano ZS (Malvern Instruments Limited, Malvern, UK). Dynamic light scattering (DLS) at 90°, with a non-invasive backscatter (NIBS) optics, was used for the measurements.
- X-ray powder diffraction (XRPD) patterns were collected by a BRUKER D8 diffractometer, using Cu-Kα radiation ($\lambda = 1.5418$ Å), filtered with a graphite monochromator. Patterns were collected in the 2θ range 2–40°, scan step 0.02°, with a counting time of 6 s $step^{-1}$.
- Thermogravimetric analyses (TG-DTG) were performed by a Perkin Elmer Q600 DTA-TG, with a heating rate of 5 °C min^{-1}, in nitrogen atmosphere, from 30 °C to 800 °C.
- Fourier transform-infrared (FT-IR) spectra of pristine and modified biochar were collected in the MID-IR region using a Thermonicolet Nexus FT IR equipped with an ATR accessory (diamond window). Analysis parameters: 100 scans, 4 cm^{-1} resolution, DTGS detector, background air.
- Raman spectra were acquired by a Jobin Yvon Labram HR800 Raman spectrometer (HORIBA Jobin Yvon, Kyoto, Japan) coupled with an Olympus BX41 microscope (Olympus Italia, Segrate, Italy) equipped with a 50X lens. The excitation line at 632.8 nm of an HeNe laser was applied. Spectra were recorded in a micro-Raman setup, placing the samples directly under the microscope lens. The laser power was set at 500 μW. Spectra were recorded by averaging three acquisitions, of 30 s each one.
- Scanning electron microscopy and energy dispersion *X*-ray spectroscopy (SEM–EDX) analyses were performed with a Zeiss EVO 50 EP (Zeiss, Jena, Germany) combined with an Oxford INCA energy 2000 spectrometer (Oxford Instruments, Abingdon, UK). The SEM–EDX was operated at an electron high tension (EHT) voltage of 15 and 20 kV, a probe current of 120 and 300 pA, and at high vacuum (about 10^{-4} Pa) conditions.
- Transmission electron microscopy (TEM) was performed using a JEOL JEM-2100Plus TEM operating with an acceleration voltage of 200 kV, equipped with an 8-megapixel Gatan Rio™ complementary metal–oxide–semiconductor (CMOS) camera. The samples were deposited onto carbon coated Cu TEM mesh grids by drop-casting dilute powder dispersions in hexane.

2.2.4 Preliminary lysozyme release tests

Preliminary LY release tests and statistical analyses were performed at pH = 3 and pH = 7 values, which simulate the stomach and gut environments, respectively. The lysozyme release was quantified by indirect competitive enzyme-linked immunosorbent assay (IC-ELISA), according to previous studies (Guagliano et al. 2023a, 2023b).

The LY release data of the two biochar carriers were analyzed with GraphPad Prism v. 9.0.0. Percentages of release of LY-CB, LY-CB-MM, LY-VB and LY-VB-MM at pH = 3 and pH = 7 were assessed by ANOVA. Post-hoc comparisons were performed using the Šidák correction. The release data of the respective biochar-LY mixtures at pH = 3 and pH = 7 were compared using Student's t-test for independent groups. The results were presented as means ± standard error. Means were considered statistically different for $p \leq 0.05$.

3 Results

3.1 Lysozyme characterization

Lysozyme was fully characterized in a previous paper by our research group (Guagliano et al. 2023b). It consists of a single polypeptide chain of 129 amino acids, with lysine at the N-end and leucine at the C-end amino acid, respectively. Lysozyme is characterized by the presence of peptide bonds between residues of amino acids, and the position of amides I, II and III are clear. In particular, Amide I is characterized by an IR band at 1665 cm^{-1}, corresponding to C = O stretching vibration, while the band at 1535 cm^{-1} corresponds to the N–H bending vibration of amide II. Lastly, bands between 1320–1230 cm^{-1} are attributable to amide III.

In the spectral region 3000–2800 cm^{-1} CH vibration modes are detectable (Zhang et al. 2017; Guagliano et al. 2023b). Thermal decomposition in N_2 (by TG-DTG analysis, Fig. S2) occurs in three main different temperature regions: (i) 23–100 °C attributed to the loss of physisorbed water on lysozyme, according to the hygroscopic properties of lysozyme; (ii) 200–600 °C, which corresponds to the larger weight loss, ascribed to the lysozyme decomposition; and (iii) 600–800 °C, due to the decomposition of the remaining organic residues (Elkordy et al. 2002).

SEM analysis highlighted smooth and spherical aggregates of diameters in the range of 4–40 μm (De S. Medeiros et al. 2014; Wu et al. 2019), while the EDX analysis

evidenced the presence of C, N, O, S and Cl (Wu et al. 2019).

3.2 Biochar (CB and VB) characterization

The elemental composition (C, N, H, S) of the biochar was determined by the EA. Results are reported in Table S2. VB and CB biochar showed a similar elemental composition, and no S was detected.

Table 1 summarizes the morphological characteristics, surface area (SA), pore volume (Vp), and pore dimension (Dp), and the granulometric analysis of the VB and CB carriers.

Both VB and CB powders have a similar trimodal distribution of the size of the particles (Table 1). Macroporosity is predominant in VB (Table 1), resulting in a low surface area, 28 m^2 g^{-1}, totally attributable to the external surface, and near to zero pore volume. On the other hand, the high surface area, 335 m^2 g^{-1}, and total pore volume 0.195 cm^3 g^{-1} of CB are the result of the contribution of micro-, and mesopore pores, with diameters in the range of 2–4 nm.

Biochar phase composition was assessed by XRPD. In the pattern of VB (Fig. 3), the reflection at 29.4 (2θ°) is strong and well-defined, and the reflections at 23, 39, (2θ°), can be associated with $CaCO_3$ calcite (JCPDS 5-586) and dolomite $CaMg(CO_3)_2$, (JCPDS01-074-1226). The broad baseline at 20–30 2θ° suggests the presence of a stacking structure of aromatic layers as a graphite-like assembly (Liu et al. 2012). A similar composition can also be inferred for CB, although Ca-containing phases are less evident.

ATR-IR spectra of VB and CB are reported in Fig. 4. There are a few weak and broad bands in the 1600–600 cm^{-1} region, namely in the range 1410–1390 cm^{-1}, and 1205–900 cm^{-1} (boxed in the figure). The 1410–1390 cm^{-1} band, which is stronger in the spectrum of VB material, is possibly due to the stretching of residual carboxylate groups and/or carbonate species. The presence of crystalline carbonate is highlighted by the two sharp bands at 870 and 710 cm^{-1} (see also the reference spectrum in Fig. 4) mainly in the VB spectrum. This is in line with the results of the XRPD.

Other broad bands in the VB spectrum around 1200 and 1000 cm^{-1} and 850–750 cm^{-1} are likely due to CO/CC stretching modes and are in line with the vibrational

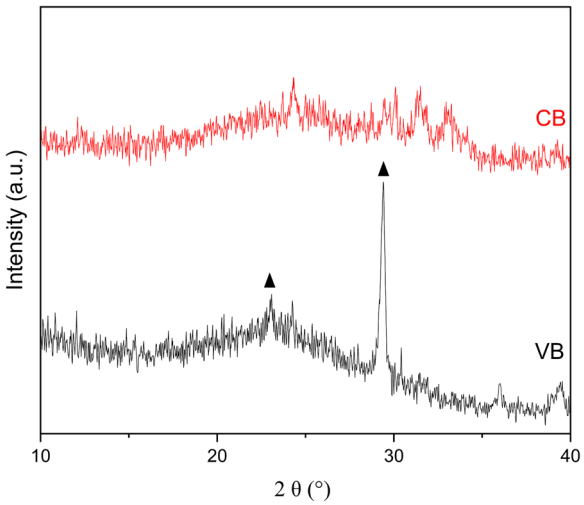

Fig. 3 *X*-ray diffraction patterns of VB (in black) and CB (in red), (▲: calcite and dolomite)

mode of cellulose residues and with the exposed functional groups containing oxygen in the biochar structure (Caporale et al. 2014).

The biomass treatment at high temperatures has removed the main part of the functional groups usually found in the composition of a complex lignocellulosic biomass, such as carboxylic groups, ketones, aldehydes and alcohols. There are only a few signals, thus demonstrating the efficiency of the pyrolysis (Brewer et al. 2014).

TG-DTG analyses of the VB and CB carriers are plotted in Fig. 5 a,b. The TG curves (Fig. 5a) of both samples show an initial thermal phenomenon, at about 100–150 °C, accounting for water evolution. This loss is more pronounced for CB than for VB, consistent with CB's high porosity. A progressive and continuous weight loss up to about 550 °C follows, probably due to the superimposition of 3.0% and 3.6% for CB and VB, respectively. Finally, a minor decomposition is faintly visible at about 650 °C.

Given the complexity of the thermal phenomena, DTG curves were also analyzed (Fig. 5b). Two temperature ranges (70–150 °C) were identified: (i) the T range = 70–150 °C, characterized by one maximum at about 72 °C; (ii) followed by a less intense range, at about

Table 1 Morphological and granulometric analysis of chestnut shell biochar (CB) and vine pruning biochar (VB)

Carrier	SA_{BET} (m^2 g^{-1})	SA_{exter} (m^2 g^{-1})	SA_{micro} (m^2 g^{-1})	Vp_{micro} (cm^3 g^{-1})	Vp_{meso} (cm^3 g^{-1})	Dp (nm)	Vp_{Total} (cm^3 g^{-1})	D10, D50, D90 [μm]
CB	335	51	284	0.125	0.07	2–4	0.195	2, 26, 75
VB	28	28	0.0	0.00	0.02	0	0.02	6, 31, 66

SA: surface area; Vp: pores volume; Dp: pores diameter; micro: micropores; meso: mesopores; exter: external; D10, D50, D90: particles dimension distribution

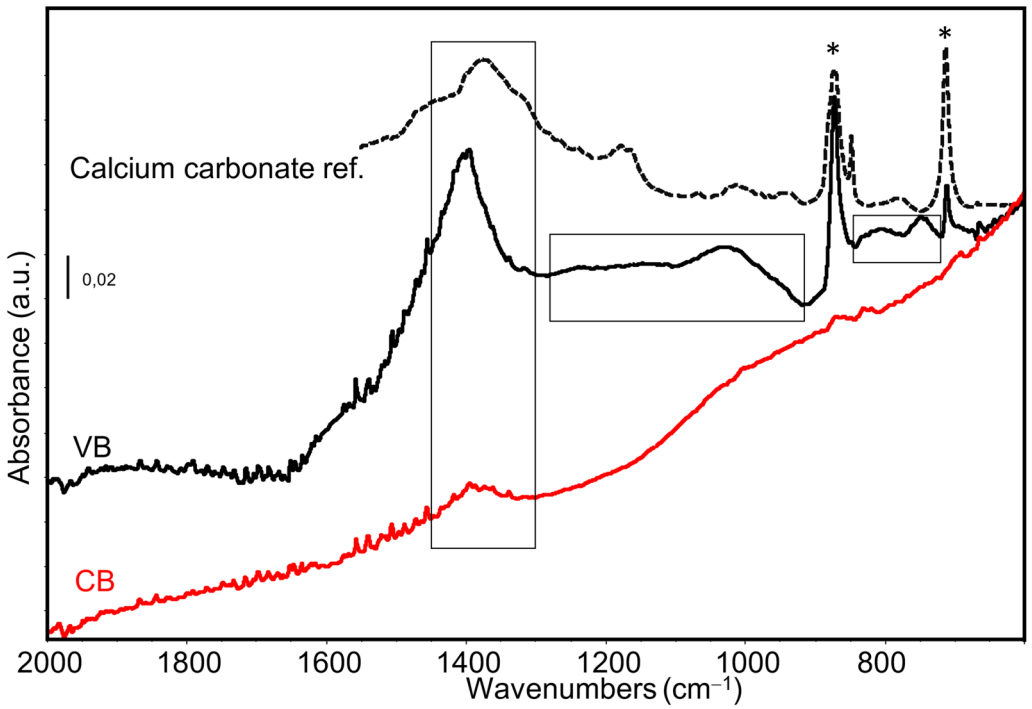

Fig. 4 ATR spectra of VB (in black) and CB (in red). Black star: carbonate species. Dashed line: reference calcium carbonate spectrum

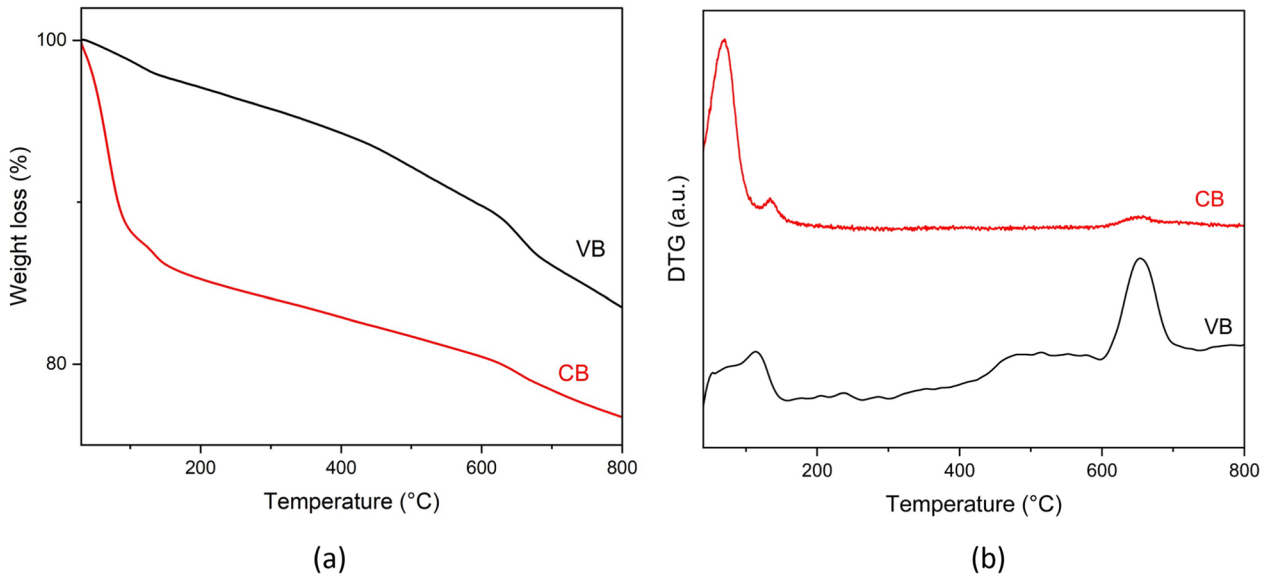

Fig. 5 **a** Thermogravimetric (TG) and **(b)** differential thermogravimetric analysis (DTG) of VB (in black) and CB (in red)

137 °C, likely due to the evolution of physisorbed water (Yi et al. 2013). Both these phenomena are more clearly evident in the CB sample.

Lastly, the phenomenon centered at 650 °C, which is more pronounced in the VB sample, is consistent with carbonate decomposition (reported at 700–800 °C), probably due to the low content and/or the poor crystallinity of this phase (Waters et al. 2017; Leng et al. 2021).

Carriers were also characterized by ZPC analysis. Negative ZPC values were found in both cases, namely, −39 mV for VB and −48 mV for CB at their pH in water (alkaline).

SEM analysis (Fig. 6a–f) revealed the high heterogeneity and morphological complexity of the powders. In both VB and CB, there is a complex network of macropores and channels (highlighted by the yellow arrows in Fig. 6b,e) (Dehkhoda et al. 2010). In line with the literature (Ma et al. 2016; Zhou et al. 2022), CB consisted of aggregates with small pores (Fig. 6a,b). On the other hand, VB showed a tubular structure, i.e., exfoliated channels, typical of lignocellulosic-based materials; sometimes characterized by cracks as shown in Fig. 6d,e (Leng et al. 2021).

EDX analysis revealed the atomic composition of the biochar. Both CB (Fig. 6c) and VB (Fig. 6f) are characterized by the presence of carbon (C) and oxygen (O), accompanied by inorganic ions which are the residue of minerals already present in the initial biomass (Ma et al. 2016; Ruiz et al. 2017).

Potassium (K), magnesium (Mg), aluminum (Al), silicium (Si), and titanium (Ti) were detected in both VB and CB. Iron (Fe) was only present in VB, while calcium (Ca), and phosphorous (P) were only detected in CB. On the basis of EDX analysis, Table 2 reports a semi-quantitative evaluation of the ionic composition.

For CB, the O/C ratio was 0.17 and for VB, it was 0.8.

3.3 The operating parameters for the hybrid biochar-lysozyme materials synthesis: contact time, pH of the initial LY solution, and lysozyme initial concentration

The effect of the operating parameters was first investigated for the VB sample, since it is a commercial product and is available in larger amounts. VB was thus considered as the benchmark. We then investigated our homemade CB carrier. All the parameters, such as the LY initial concentration, the contact time, and initial pH, were studied in order to reach a final LY loading of 21–23 $mg_{LY}\ g_{Carrier}^{-1}$. This load is considered sufficient for a final application (Oliver et al. 2014), and corresponds to

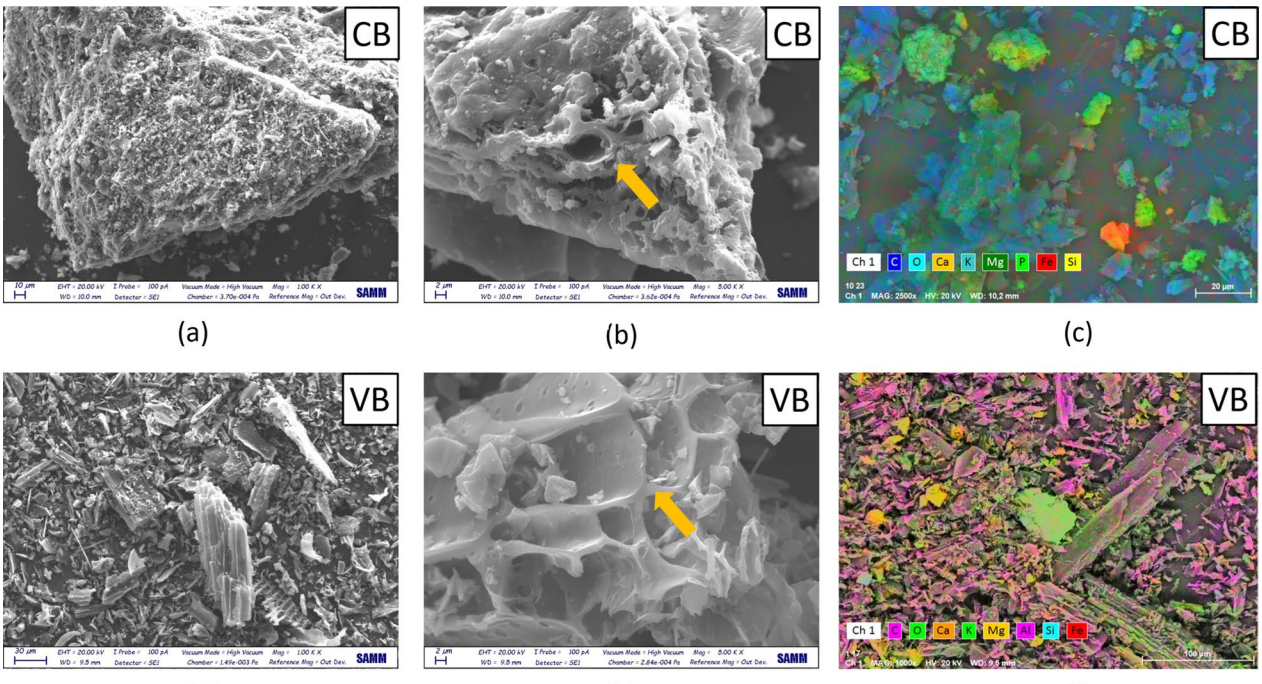

Fig. 6 SEM images of CB (**a**, **b**) and its EDX map (**c**); SEM images of VB (**d**, **e**) and its EDX map (**f**). SEM image magnification: 1000 X (**a**), and (**d**); 5000 X (**b**) and (**e**). The complex network of macropores and channels are highlighted by the yellow arrows

Table 2 Semi-quantitative analysis (by EDX) of chestnut shell biochar (CB) and vine pruning biochar (VB)

CARRIER	C (%)	O (%)	O/C	Mg (%)	Al (%)	Si (%)	K (%)	Ti (%)	Fe (%)	Ca (%)	P (%)
CB	82	14	0.17	0.29	0.04	0.1	1.48	0	0	1	0.01
VB	40	34	0.85	3.21	6.54	7.09	1.09	0.11	7.89	0	0

[Data expressed in Atomic concentration (%)]

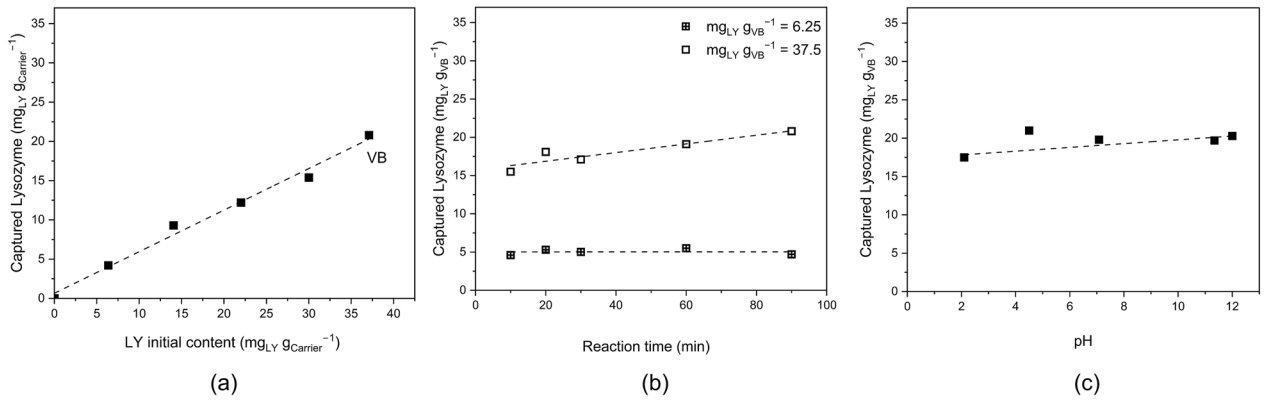

Fig. 7 Adsorbed LY on VB as a function of: (**a**) initial lysozyme content, (**b**) reaction time, and (**c**) pH of the initial lysozyme solution

approximately 168–184 mg of lysozyme, in feed supplemented with 2% biochar—on the basis that a weaned piglet (28 days of age) consumes between an average of 400 g (until 28 days) and 900 g (near 42 days) of feed daily. Figure 7a–c reports the results in terms of captured LY.

The effect of the initial LY content was verified in the range 6.25–37.5 mg_{LY} $g_{Carrier}^{-1}$ range (corresponding to 0.25–1.5 mg mL^{-1}) at the initial natural pH of the LY solution (4.5–4.7), and by fixing the contact time at 90 min (Guagliano et al. 2023a). Figure 7a highlights a linear dependence between the LY loading and the initial LY concentration. In these conditions, the target LY loading of 21 mg_{LY} g_{VB}^{-1} is reached for an initial LY concentration of 37.5 mg_{LY} g_{VB}^{-1}, corresponding to a reaction yield of 56%.

The effect of contact time was then analyzed in the range 10–90 min, and for two different LY initial contents, high (37.5 mg_{LY} g_{VB}^{-1}) and low (6.25 mg_{LY} g_{VB}^{-1}); see Fig. 7b.

A negligible or no influence of the contact time was found. The total LY uptake was already reached in 10 min, for 6.25 mg_{LY} g_{VB}^{-1}, and only a slight uptake increase was observed for 37.5 mg_{LY} g_{VB}^{-1}. Therefore, to ensure the maximum LY loading, at any initial LY concentration, further experiments were performed by fixing the contact time to 90 min. Selected experiments were performed twice and standard deviation of ± 1.5 mg_{LY} g_{VB}^{-1} was calculated.

Finally, the effect of the initial pH of the LY solution was checked by fixing the LY initial content at 37.5 mg_{LY} $g_{Carrier}^{-1}$ and reaction time at 90 min (Fig. 7c). pH variation was performed by the addition of sodium hydroxide (NaOH) and nitric acid (HNO_3). Five pH values were tested, namely 2.0, 4.5–4.7, 7.1, 11.3 and 12.0. Among the selected pH values, 4.5–4.7 corresponds to the natural pH of the LY solution and 11.3 corresponds to the LY pKa. No or a negligible pH effect on LY final loading was found in the pH range considered (Fig. 7c).

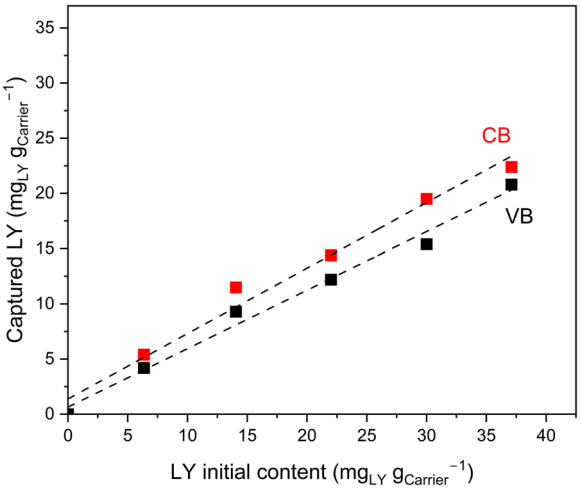

Fig. 8 LY capture as a function of the initial LY contents for CB (red squares). VB for comparison (black squares)

The following operating conditions were selected as optimal for the preparation of a biochar-based material containing about 21–23 mg $_{LY}$ $g_{Carrier}^{-1}$: contact time of 90 min, RT, stirring at 500 rpm, initial content 37.5 mg_{LY} $g_{Carrier}^{-1}$, and no pH correction.

The selected conditions were then validated using CB to evaluate the effect of the biochar material and to generalize the experimental approach.

The effect of the biochar was assessed by performing the adsorption reaction, and applying the same experimental conditions that had been used for VB, and exploring the same range of initial LY contents, i.e., 6.25–37.5 mg_{LY} g_{CB}^{-1}. Figure 8 shows the results, where the VB curve is reported for comparison. CB also behaved linearly, suggesting that similar capture mechanisms are

active for both carriers. Very close final LY loadings were obtained, 21 and 23 $mg_{LY}\ g_{Carrier}^{-1}$, for VB and CB, respectively.

In conclusion the experimental approach (solid/liquid reaction) and the experimental parameters (90 min of contact time, RT, stirring at 500 rpm, an initial LY content in solution of 37.5 $mg_{LY}\ g_{CB}^{-1}$, and no pH correction) would appear to be effective in reaching a LY loading target of 21–23 $mg_{LY}\ g_{Carrier}^{-1}$.

3.4 The lysozyme-carrier interaction

LY-VB with the LY loading of 21 $mg_{LY}\ g_{VB}^{-1}$ and LY-CB with the LY loading of 23 $mg_{LY}\ g_{CB}^{-1}$, were fully characterized. The XRPD patterns (Fig. S3) did not reveal any major differences between the pristine carrier and the hybrid materials. The phase composition and the phase crystallinity, already detected in VB and CB, were preserved in the corresponding functionalized materials. In the LY-VB sample, the reflections associated with $CaCO_3$ calcite (JCPDS 5–586) and dolomite $CaMg(CO_3)_2$, (JCPDS01-074–1226) are still manifest, and they are still less evident in LY-CB. In the LY-VB sample there was again a broad modulation of the base line, at 20–30 2θ°, which was associated with the presence of a graphite-like structure (Liu et al. 2012).

The thermal analysis was also performed for the hybrid samples, (Fig. S4). As reported for the pristine carriers, water evolution was first detected, followed by a progressive and continuous weight loss of up to about 550 °C, and a further decomposition at about 650 °C. The weight loss between 250 and 550 °C accounted for approximately 4.5% for LY-VB and 3.0% for LY-CB, which was very close to those of the pristine carrier (3.6% for VB and 3% for CB). It is thus difficult to distinguish between the various decomposition phenomena in pristine and hybrids materials. In fact, not even the DTG analysis was able to provide more information on the presence or amount of LY in the samples (Fig. S3b). These inabilities could be due to the low LY content in the samples, and/or with a high dispersion of the LY molecules, which may have interacted strongly with the carrier.

FTIR spectra of the biochar after LY adsorption showed very weak additional features due to the organic component. Figure 9 therefore reports the subtraction spectra [composite]—[reference biochar] in order to enhance the intensities of the most significant features. In the LY-VB spectrum, lysozyme characteristic bands were clearly detectable at 1645 and 1550 cm^{-1}. These correspond to amide I and amide II vibrational modes, which were only slightly shifted in comparison with the bands of the pure protein reported in the same Fig. (1642 and 1520 cm^{-1}). This small shift may indicate H-bond interactions with the biochar surface. The negative band below 1400 cm^{-1} suggests that some surface species, namely carbonates, are replaced during LY adsorption. Lastly, the broad

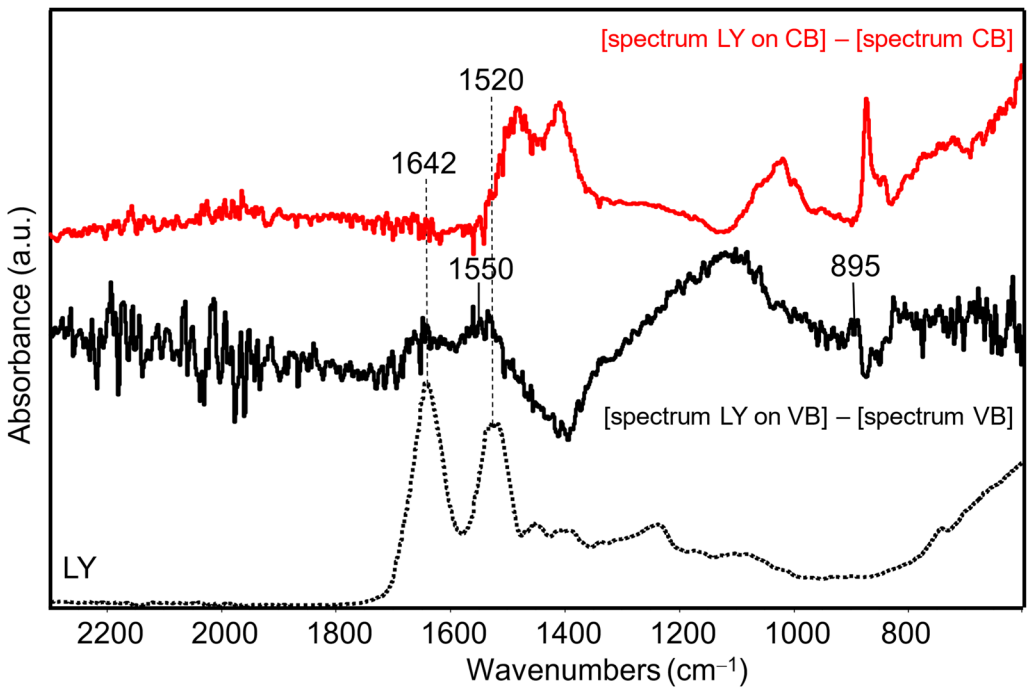

Fig. 9 FT-IR spectra of pristine LY (dotted line), subtraction spectrum [(LY-VB)-VB] (black), and [(LY-CB)-CB] (red)

absorption at 1100 cm^{-1} could be due to some CO/CC stretching modes of the interacting protein (Barth 2007).

On the other hand, LY-CB spectra (Fig. 9) revealed the formation of new bands at 1485, 1415, 1025 (complex) and 872 cm^{-1}. Some of these bands can be assigned to residual carbonate species (i.e. the band at 872 cm^{-1}), while bands in the range 1500–1400 cm^{-1} could be related to exposed carboxylate groups and/or LY diagnostic bands that had been strongly affected by the interaction with biochar and had greatly shifted to lower frequencies. The disappearance of amide I and II bands following enzyme immobilization possibly confirms the binding between the protein and the biochar structure, which involves the interaction of amino-groups of the organic moiety (González et al. 2013).

Considering the impossibility to obtain definite and direct evidence of the LY allocation for both LY-VB and LY-CB, by FT-IR, a further characterization was performed with Raman spectroscopy (Fig. S5 a,b).

Although Raman spectra are quite noisy, the particular characteristics of biochar are pinpointed by the two bands approximately at 1300 cm^{-1} (D band) and 1600 cm^{-1} (G band) (Yan et al. 2021).

The D band is associated with disordered carbon structures, whilst the G band is related to the vibration of sp2-hybridized carbon atoms in graphitic carbon layers, which are present in biochar, as also confirmed by XRPD analysis. The distinct and sharp peaks also indicate a high degree of carbon ordering, in line with the pyrolysis temperature. However, no changes in the D and the G bands of the biochar were detected in the presence of LY molecules (Fig. S5a), and only very small differences were found when magnifying the 3500–2000 cm^{-1} zone, which are typical of C-H stretching (Fig. S5b). In LY-CB, there was a slight increase in the intensity of this broad and noisy band, which suggests that some adsorption of organic compounds has occurred, but without any direct confirmation of the presence of LY.

The presence of LY in LY-CB, which is the sample of most interest, was also verified by SEM–EDX analysis (Fig. 10a, b). In fact, in our previous work, the detection of sulfur (S) by EDX was found to be an efficient technique for LY detection, as it is present in the biomolecule (Guagliano et al. 2023a, 2023b).

In the complex morphology of LY-CB (Fig. 10a), it is difficult to discriminate between features of the carrier and those of lysozyme, as the typical LY spherical particles were no longer detected (Fig. S6). However, the EDX analysis showed a homogeneous and well-dispersed S distribution on the carrier's particles (Fig. 10b). On the other hand, no or negligible S amounts were found in the EDX of the pristine CB carrier, thus confirming the presence of LY which seemed to be well dispersed on biochar.

To further explore the LY-carrier interactions, characterization results regarding synthesized hybrid samples (LY-VB and LY-CB) were compared with those of a mechanical mixture of the components in the same LY/biochar ratio of the hybrid samples. Two samples were prepared (LY-VB-MM and LY-CB-MM), which were fully characterized and compared with the corresponding LY-VB and LY-CB obtained via the solid/liquid reaction.

Despite the same LY loading of the hybrid materials, LY decomposition in the mechanical mixtures was more evident in the DTG analysis. In fact, the thermal phenomenon, with associated weight loss, which occurred in the T range 250–450 °C, and reached a maximum at 300 °C, corresponds to free LY decomposition (Fig. S7). The broadening and slight anticipation of the phenomenon, suggested the presence of less dispersed LY molecules,

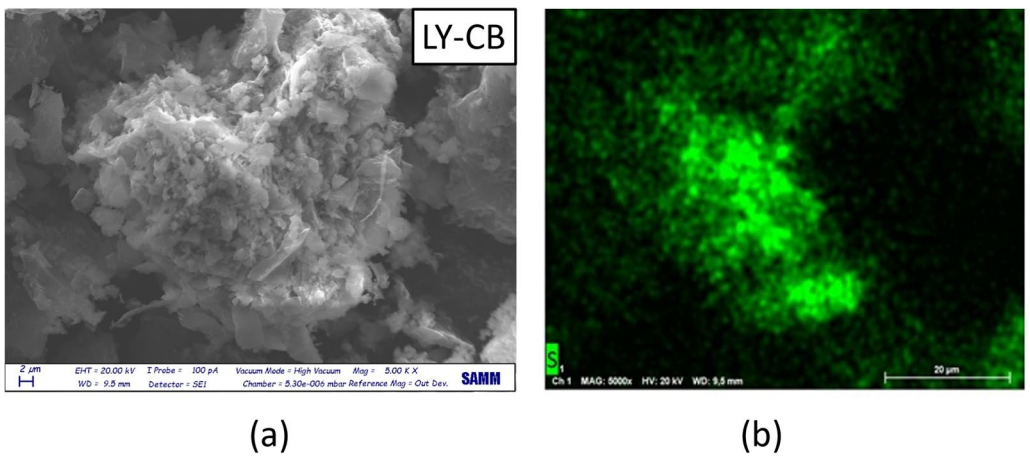

Fig. 10 SEM–EDX images of LY-CB particles: (**a**) SEM image and (**b**) sulfur distribution by EDX

which however, were perhaps weakly interacting with the carriers.

Therefore, the absence of LY decomposition in the DTG of the hybrid materials, LY-CB and LY-VB (Fig. S4), could be further evidence that the LY is well dispersed in these samples.

The CB-based hybrid and mechanical mixture samples were further investigated by FTIR (Fig. 11) and SEM–EDX analysis (Fig. 12).

FTIR spectrum of the mechanical mixtures (Fig. 11, sample LY-CB-MM) showed that the main bands were almost unchanged, due to pure LY at 1640 and 1520 cm^{-1} (amide I and amide II bands, respectively). A broad absorption was also detected in the range 1250–1000 cm^{-1}, likely due to a mixture of CC and CO bonds of organic and carbonate species. Interestingly, this spectrum is different from that of the hybrid materials (LY-CB shown in Fig. 11 as a comparison to LY-CB-MM), where LY bands are significantly modified and shifted in position. These findings are in agreement with the Raman analysis and microscopies results discussed below.

Raman spectroscopy (Fig. S8) also evidenced LY in the mechanical mixture, characterized by weak Raman shifts in the range 3000–2800 cm^{-1} corresponding to CH stretching modes (Chen et al. 2019). LY Raman signals were more easily distinguishable in LY-CB-MM than in the hybrid samples. Again, spectroscopic results suggested that LY was less dispersed (Kocherbitov et al. 2013) in the mechanical mixture, which was better explored by SEM–EDX analysis (Fig. 12).

The absence of LY aggregates, as well as the presence of a homogeneous S distribution in the hybrid material (Fig. 12a) further suggest the occurrence of a potentially stronger LY-biochar interaction due to the adsorption method. In contrast, the typical LY spherical particles in the mechanical mixtures (about 10 µm, Fig. 12b) and the localized areas with a higher sulfur content, confirmed the hypothesis of poorly dispersed LY molecules in the chestnut biochar.

To gain a deeper insight into the distribution of the lysozyme on the carrier's surface, TEM images were collected on VB, LY-VB and LY-VB-MM (Fig. 13a–c), as well as on CB, LY-CB and LY-CB-MM (Fig. 13d–f).

TEM images of both bare biochar (Figs. 13a and d) show large sheet-like shape particles with an average size of between 2–5 µm. In both samples, fewer particles and smaller aggregates (< 200 nm) were detected, as well as rod-like structures, which suggest an intrinsic heterogeneity of the materials.

After the addition of LY through the mechanical mixture method, new particle aggregates became evident (Fig. 13b and e) on the surface of the sheet-like particles of both VB and CB, with an average size of 200–300 nm. These were non-homogeneously distributed all over the sample and were likely due to LY aggregation phenomena on the biochar surface.

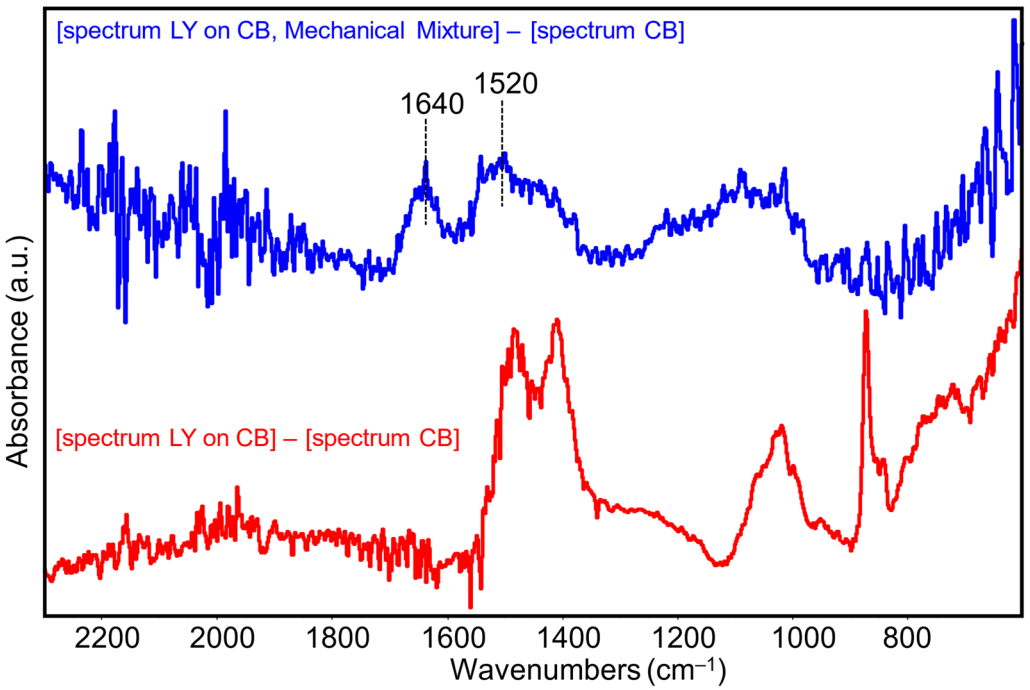

Fig. 11 Comparison of hybrid solid LY-CB and the corresponding mechanical mixture LY-CB-MM as representative sample using FTIR

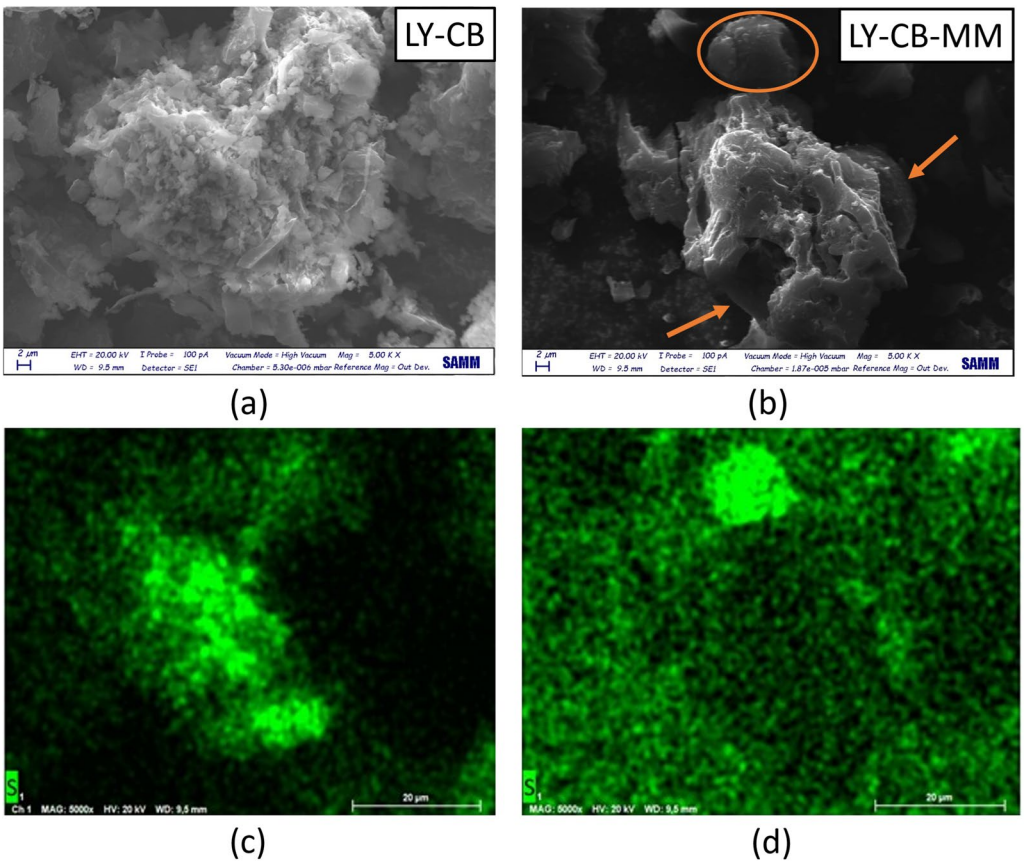

Fig. 12 SEM–EDX analysis of LY-CB (**a**) reported for comparison, and LY-CB-MM (**b**). Orange circles and arrows: LY aggregates. In green the S distribution in the two samples (**c**, **d**), detected by EDX analysis

In contrast, when LY was added by the solid/liquid adsorption procedure, layers of organic material (~ 50 nm thickness, Fig. 13c and f) appeared on the extended surface areas of the biochar (> 1 µm). These can be ascribed to an improved LY dispersion on the biochar particles, although again the overall dispersion in the sample was not completely homogeneous as bare biochar particles were also detected.

In general, the morphology of the biochar was not modified either by the mechanical mixing or the solution mixing. The only exception was for CB-LY-MM, where additional structures of about 100 nm and with an intrinsic porosity were observed (Fig. 13e, highlighted by a yellow arrow). These structures are characterized by mesoporous channels with a diameter of a few nanometers (average diameter 4 ± 1 nm) and may be generated by the disruption of CB aggregates in the bare sample.

3.5 Preliminary lysozyme release assay of lysozyme

The adsorption and release processes of lysozyme are shown in Fig. 14. The percentages of released LY at pH = 3 and pH = 7 are plotted in Fig. 15, where the behavior of the two synthesized LY-biochar samples is compared with the corresponding mechanical mixture.

At pH = 7 the released lysozyme corresponded to 0.23 $mg_{LY}\ g^{-1}$ for CB and 0.44 $mg_{LY}\ g^{-1}$ for VB. LY-VB-MM showed a significantly higher release of LY for both pH = 3 and pH = 7 compared to all the other treatments ($p < 0.001$). LY-CB showed a lower release of LY at pH = 3 compared to LY-CB-MM and LY-VB ($p < 0.01$). LY-CB also exhibited a lower release compared to LY-VB ($p < 0.001$), but with a comparable percentage to LY-CB-MM at pH = 7.

Considering each CB and VB mixture individually, the release of LY at pH = 7 was higher compared to pH = 3 ($p < 0.05$), except for LY-CB-MM, which showed a significantly lower release of LY at pH = 7 compared to pH = 3 ($p < 0.05$).

4 Discussion

4.1 Physico-chemical properties of carriers

The physico-chemical properties of biochar mainly derive from the combined effect of the composition of the biomass feedstock and the pyrolysis temperature (Leng et al.

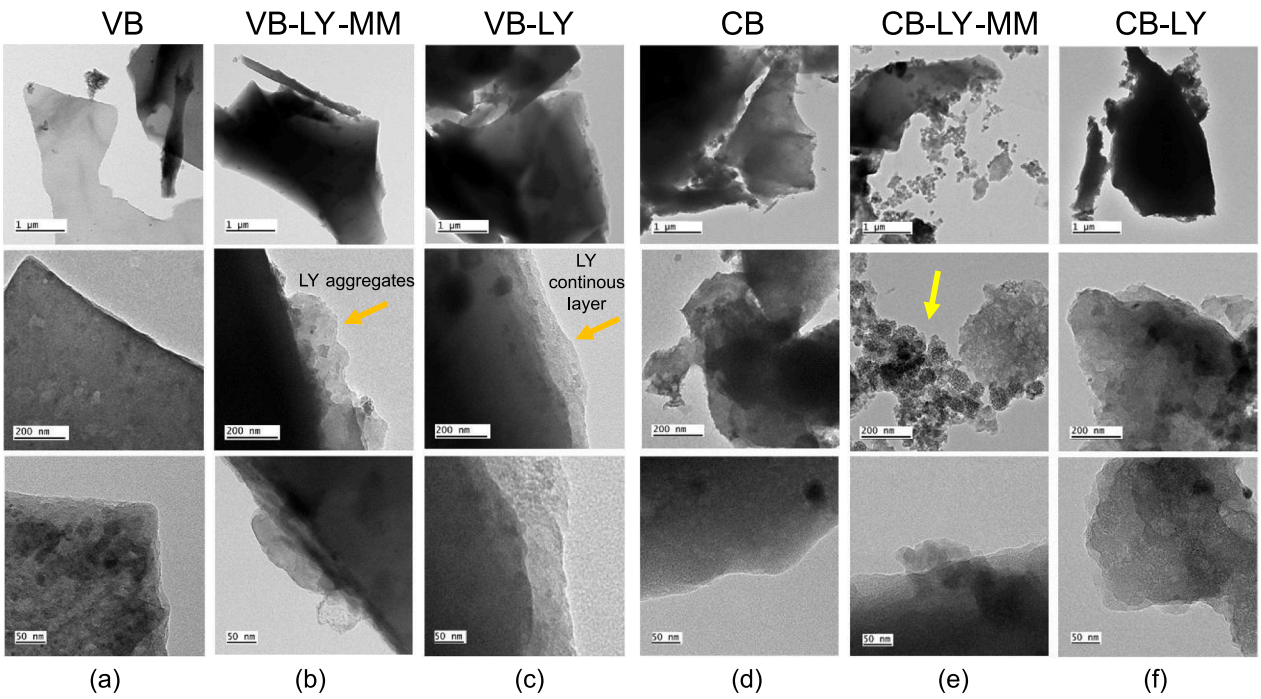

Fig. 13 TEM images of (**a**) pristine VB, (**b**) LY-VB-MM, and (**c**) LY-VB, (**d**) pristine CB, (**e**) LY-CB-MM, and (**f**) LY-CB at three different magnifications. Orange arrows indicate LY in the mechanical mixture and in the hybrid material obtained through solid/liquid adsorption. The yellow arrow indicates the formation of an additional structure in LY-CB-MM

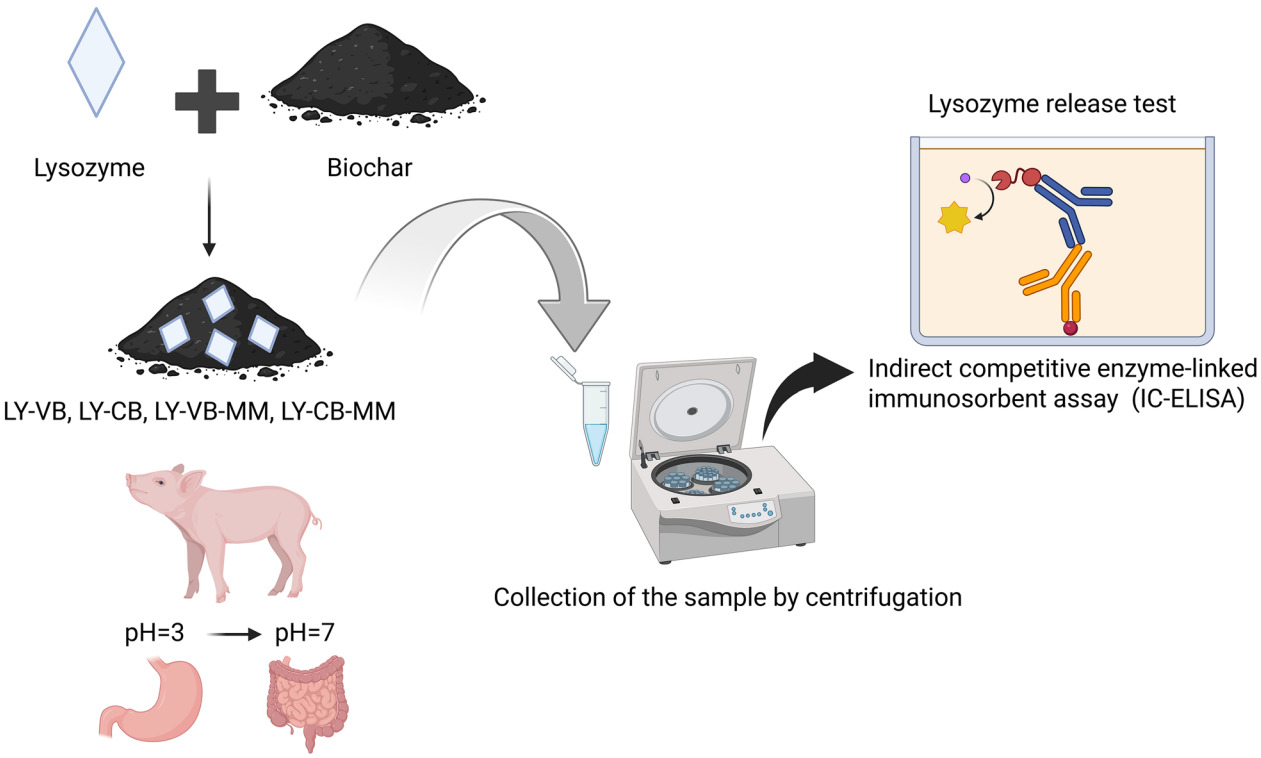

Fig. 14 Procedures of adsorption and release of lysozyme Created in BioRender. Guagliano, M. (2026). https://BioRender.com/rkz4ygt

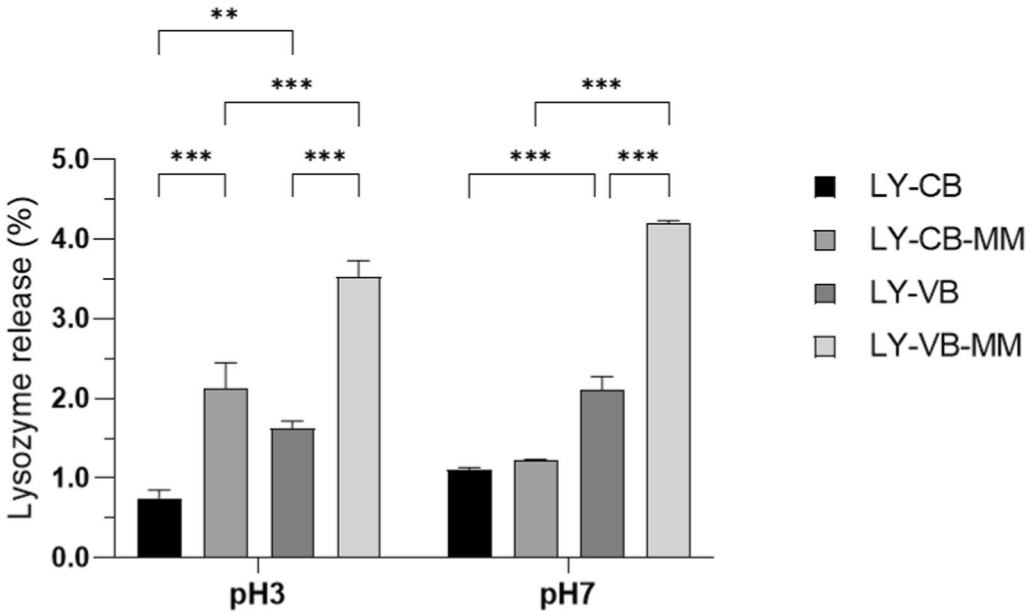

Fig. 15 LY Release percentages (w/w) for LY-CB, LY-VB and the corresponding mechanical mixture (LY-CB-MM and LY-VB-MM) at pH = 3 and pH = 5. Data are presented as means ± standard error. *Asterisks indicate statistically significant differences among groups within the same pH conditions (**indicates $p < 0.01$; ***indicates $p < 0.001$). Statistical analysis was performed using ANOVA to compare each group mean. "*p*" indicates the *p-value,* also known as the "observed significance level" for the test hypothesis

2021). Different feedstocks can contain several inorganic ions, such as alkali and alkali earth metals, which produce different contents of ash during the thermochemical process. A high ash content, which leads to pore blockage, results in fewer micropores, hence a lower surface area. On the other hand organic molecules, which release high volatile matter, promote the formation of micropores and a higher surface area (Leng et al. 2021).

For lignocellulosic biomass (e.g. the VB and CB feedstocks) lignin, cellulose, and hemicellulose are the main components, and are characterized by different decomposition temperatures (hemicellulose 220–315 °C, cellulose 315–400 °C, and lignin 160–900 °C) (Yang et al. 2007). The thermochemical conditions are therefore the controlling decomposition parameters during the process. The widely different morphological properties of VB, (28 m^2 g^{-1}) and CB, (335 m^2 g^{-1}), strongly depend on the process temperature, such as 600–800 °C for CB (Fig. S1) and 450–500 °C for VB.

However, it is important to point out that lower temperatures do not lead to a complete volatilization of the constituents. As a result pore blockage can occur and/or the formation of new pores may be hindered (Zhang et al. 2013; Pallarés et al. 2018) which in this case, led to a lower surface area of the VB biochar.

Moreover, considering that the gasification temperature of CB (600–800 °C) was higher than that of the pyrolysis of VB (450–500 °C), a lower surface area and larger pores would seem to be justified for VB (Leng et al. 2021). According to Ma et al. 2016; and Batista et al. 2018, the O/C ratio, calculated by EDX, provides information on the degree of carbonization. The greater carbonization of CB, O/C = 0.17, compared with O/C = 0.8 of VB, together with higher ash content are consistent with the aforementioned pore clogging effect (Yuan et al. 2011; Ruiz et al. 2017; Nunes et al. 2021). This determines the very low pore volume (0.02 cm^3 g^{-1}), as well as the low surface area (28 m^2 g^{-1}) of VB, which was accountable only due to the external surface area.

The process temperature is also responsible for ZPC values of VB and CB (Yuan et al. 2011; Batista et al. 2018; Hong et al. 2019). Nevertheless, biochar obtained at higher temperatures should show a less negative zeta potential, mainly due to the decomposition of most of the organic moieties, VB. However, which was obtained at a lower temperature than CB, showed a less negative ZPC (−39 mV) than CB (−48 mV).

4.2 Effect of the synthesis parameters

The experimental conditions adopted, consisting of 90 min of contact time, 37.5 mg_{LY} $g_{biochar}^{-1}$, and initial pH = 4.5–4.7, led to LY loadings of 21–23 mg_{LY} $g_{Carrier}^{-1}$, which is the LY value considered sufficient for the final application (Oliver et al. 2014). The uptake reaction was quite fast at all of the initial LY concentrations, and the reaction was almost completed within the first

10–15 min. The initial LY content was the only parameter governing the capture reaction, in fact the LY adsorption reaction showed a linear trend with the concentration of LY in solution. Conversely, the pH of the initial LY solution did not affect the reaction performance, and a constant LY loading was always obtained. However, a large initial pH range (2–12) was applied. This result can be traced back to the reported buffer capacity of the LY in water solution (Kim and Myerson 1994). LY appears to be always positively charged (Wu et al. 2019), both at a pH of 4.5–4.7, which is natural value, and at pH 8.8–9, the value of the final reaction. The capture mechanism and the adsorbate-carrier interaction can therefore occur via the same mechanism and to the same extent at any of the pH conditions applied here (Wu et al. 2019).

4.3 Lysozyme-carrier interaction

The mode and strength of the lysozyme-biochar interaction, such as the protection and the modulated supply of the active biomolecule to the animal, are fundamental parameters for the final application.

This interaction depends on the nature of the carrier. There are various contributing factors such as the morphology, surface functional groups, and/or surface charge (Pandey et al. 2022; Guagliano et al. 2023a), along with the LY molecular dimension charge, structural conformation and steric hindrance (Noritomi 2019).

The characteristics of the carriers mainly derive from the primary feedstock and the pyrolysis temperature, while those of the LY depend primarily on the contacting reaction conditions.

It is clear that the morphology did not influence the LY capture behavior. Despite VB and CB showing very different morphologies (see Table 1), the same LY total loading, 21–23 $mg_{LY}\ g_{Carrier}^{-1}$, was achieved upon the reaction, thus highlighting that there is no direct correlation between the loading and the morphology of the carriers.

Similar results have been reported regarding many different carriers and biomolecules. For instance, González et al. 2013 found that biochar with SA of 0.1 $m^2\ g^{-1}$ and a particle size of between 53 µm and 90 µm could immobilize 99.4–100.4 $\mu g\ g^{-1}$ of lipase. On the other hand, others have reported that the capture of polygalacturonate and cellulase on biochar is not dependent on the carrier surface area or on any other morphological characteristics of biochar (Jaiswal et al. 2018). Lastly, the same behavior was found when LY was immobilized on inorganic carriers, such as mineral clays or zeolites (Guagliano et al. 2023b), when applying the same procedures and conditions of this work.

The LY-carrier interaction did not seem to be influenced by pore filling. In fact, the CB porosity is predominantly the result of the micropores (Dp = 2–4 nm), which hinder the allocation of lysozyme (4.5 × 3.0 × 3.0 nm, Cegielska-Radziejewska et al. 2008).

The absence of LY adsorption inside the pores is also supported by comparing the external surface areas of the carriers, i.e. 51 $m^2\ g^{-1}$ for CB and 28 $m^2\ g^{-1}$ for VB. The close similarity of these values could suggest a preferential LY-biochar interaction at the external surface area, thus explaining a comparable uptake behavior. Accordingly, not all the measured BET surface area of CB (335 $m^2\ g^{-1}$) is available for the LY binding process.

In addition, as no structural or phase composition modifications were observed in the XRPD patterns of the pristine VB and CB upon LY adsorption, it can be hypothesized that LY molecules are located preferentially at the external surface of the biochar through electrostatic interactions, which is the most probable approach for the adsorption of organic molecules onto biochar (Alsawy et al. 2022). This hypothesis is supported by the negative ZPC values of the carriers (−48 mV for CB and −39 mV for VB) and the positive ZPC of LY under reaction conditions (pH between 8.8–9) that highly favor charge interactions.

In fact, such interactions have already been reported and proved on samples of different compositions, but carried out via the synthetic approach reported here, i.e., solid/liquid adsorption (Cristiani et al. 2021; Guagliano et al. 2023b).

Some indications regarding the nature of the LY interaction with the surface groups of the biochars were obtained by FTIR and Raman spectroscopies. In the FTIR spectrum of LY-VB hybrid material, peaks due to carbonates, oxygenate functional groups from, possibly, cellulose residues, were detected together with additional very weak IR bands due to LY (Fig. 11). The CB sample, on the other hand, showed almost no IR feature of functional groups, and, in the spectrum of the corresponding hybrid material, IR bands directly attributable to LY disappeared or changed in shape and position. This effect could be due to a strong interaction of the enzyme with the biochar structure. Raman spectroscopy of the LY-CB hybrid did not show changes in the D and the G bands of the biochar, i.e. 1300 and 1600 cm^{-1}, which were still detectable in the presence of LY (Fig. 12). Only a very low increase in intensity of the broad and noisy band typical of the C–H stretching (3500–2000 cm^{-1}) was detected, which could be associated with the enzyme structure. In comparison, IR and Raman spectra of the LY-CB mechanical mixture were well evidenced by the typical bands of LY, which, however, were not affected by immobilization. A significant interaction between the enzyme and CB can thus be hypothesized, although it is difficult

to connect it to the nature of the sites involved in the interaction.

A surface lysozyme-carrier interaction in the synthesized samples was confirmed by SEM–EDX analysis, in which there were no spherical aggregates—this is typical of free LY (Guagliano et al. 2023a, 2023b). The homogeneous distribution of S atoms on the carrier particles (Fig. 15b) proved the homogeneous dispersion of the biomolecules on the carrier surface (Guagliano et al. 2023a, 2023b).

Finally, TEM analysis, in line with both SEM–EDX and TG-DTG results, seems to confirm the LY interaction with the biochar surface. In the LY-VB and LY-CB samples, there was a clear homogeneous and continuous LY coverage of the biochar surface, due to a possible stronger interaction induced by the synthetic approach. In contrast, in LY-VB-MM and LY-CB-MM, LY seems to form aggregates that were observed at the edge of the material, which indicates a different and less efficient interaction with the surface, and thus possibly a weaker interaction.

4.4 Controlled release of lysozyme

The gastrointestinal environment in swine species exhibits a wide range of pH levels. Following ingestion, the bolus undergoes an acidic environment characterized by a low pH (typically = 3) (Ange et al. 2000; Mößeler et al. 2010). Subsequently, pH levels increase after passing through the pylorus into the gut, where pH values reach neutrality or slight alkalinity (7–8) (Henze et al. 2021). Developing efficient carriers for targeted delivery should lead to an effective and precise release of molecules at the specific site where they are intended to exert their beneficial or therapeutic effects (Pawar et al. 2014). In our study, we developed a biochar-based carrier for bioactive molecules for functional nutrition using lysozyme as a protein model due to its important antimicrobial activity and molecular weight.

Lysozyme release showed a pH-dependent behavior. In hybrid samples higher release percentages were achieved at pH = 7. This suggests that the carrier facilitates the release of lysozyme in the simulated gut environment. Although the overall release rates were modest (< 10%), the improved performance at pH = 7 highlights the potential for targeted supplementation with small quantities of bioactive molecules. In the mechanical mixture, a higher release was observed for both pH = 3 and pH = 7 compared to the solid/liquid adsorption, thus indicating that in the mechanical mixture the process is not controlled. The solid/liquid adsorption therefore appears more suitable for functionalizing biochar with bioactive molecules such as LY.

5 Conclusions

Our experimental approach enabled us to find the optimal conditions for the effective capture and immobilization of lysozyme by biochar obtained from different residual sources (vine pruning, VB, and chestnut shells, CB).

The solid/liquid reaction between lysozyme and biochar was quite fast and the maximum loading of 21–23 $mg_{LY}\ g_{Carrier}^{-1}$ was reached within 90 min of stirring 1.5 mg mL^{-1} of initial lysozyme at a pH 8.8–9, at room temperature with a reaction yield of 50–60%.

Lysozyme total loading was not affected by the biochar morphology, since carriers characterized by different surface areas in terms of one order of magnitude were able to load the same amount of lysozyme. In addition, the zero-point charge of the carriers influences the adsorption process, more than surface area, since the LY–carrier interactions are essentially due to charges of opposite signs.

The synthetic route proposed facilitates both biomolecule protection and potential controlled release in the different tracts of the intestinal environment. In fact, in the hybrid materials, thanks to the synthetic approach, the LY molecules seem to be more strongly bonded to the biochar surface. It is also possible they are interacting with surface residual functional groups, and therefore, the homogeneously dispersed LY results in the pH-dependent release observed. This behavior only partially occurs in the mechanical mixture, where the interactions are weaker.

Our results suggest that biochar has an interesting potential as a carrier for the release and delivery of bioactive molecules in conditions that simulate the intestinal environment and thus, can facilitate the design of functional diets for animal nutrition with a translational potential for the production of nutraceuticals.

6 Final considerations

The supplementation of biochar-protected LY is promising, and could increase the opportunities for targeted delivery and release of various bioactive molecules into the gastrointestinal tracts in the formulation of functional diets. Our study thus represents a step forward in precision livestock farming aimed at supporting the sustainable growth of the farming sector in accordance with One Health principles.

However, several aspects still need clarification, for instance, whether the enzyme retains its activity across different pH levels, and whether enzymatic hydrolysis by

endogenous gastric enzymes could influence or modulate its activity.

Further studies are needed to evaluate the stability of the enzyme after adsorption and following release under varying pH conditions, using techniques such as circular dichroism (CD) and fluorescence spectroscopy.

The nature of the interaction between the enzyme and the biochar is also still not fully understood, and targeted studies are needed. Finally, dedicated in vivo studies should be conducted to evaluate the long-term safety of the biochar use.

However, the use of biochar as a carrier can be considered a step forward in a competitive bioeconomy for a sustainable future. The revaluation of biochar, i.e. the "waste" of a near-zero-emission energy production, by its transformation into a bio-based advanced material, fosters the principles of circularity and environmental sustainability, including climate neutrality and zero pollution objectives, in the context of the European Green Deal.

Supplementary Information

The online version contains supplementary material available at https://doi.org/10.1007/s42773-025-00557-w.

Supplementary Material 1.

Acknowledgements
The authors would like to gratefully acknowledge Romagna Carbone (Bagnacavallo, Italy), for supplying the vine pruning biochar. Thanks are also due to Prof. Luigi Brambilla (FunMat Lab—Politecnico of Milano, Dipartimento di Chimica, Materiali ed Ingegneria Chimica "Giulio. Natta", Italy) and Andrea Basso Peressut (Mat4En2 lab- Politecnico of Milano, Dipartimento di Chimica, Materiali ed Ingegneria Chimica "Giulio. Natta", Italy) for the Raman analysis. Thanks also to Ana Bahamonde (Instituto de Catalisis y Petroleoquimica, CSIC, Spain) for her help in the interpretation of the BET analysis results. Lastly, the authors would like to thank Mattia Ronchi (SAMM Lab—Politecnico of Milano, Dipartimento di Chimica, Materiali ed Ingegneria Chimica "Giulio. Natta", Italy) for his help in performing the scanning electron microscopy (SEM) and energy dispersion X-ray (EDX) analyses. Marianna Guagliano also gratefully acknowledges the European project PON FSE REACT-EU, and the resources allocated by Ministerial Decree No. 1061 of 10 August 2021.

Author contributions
Marianna Guagliano: Data curation, conceptualization, methodology, validation, investigation, writing original draft, writing—review & editing. Serena Reggi: Methodology, validation, investigation, writing—review & editing. Matteo Dell'Anno: Conceptualization, methodology, validation Writing—review & editing. Silvia Mostoni: methodology, investigation, writing—review & editing. Filippo Ottani: methodology, formal analysis. Simone Pedrazzi: methodology, formal analysis. Marco Puglia: methodology, formal analysis, writing—review & editing. Giovanni Dotelli: formal analysis. Luciana Rossi: conceptualization, writing—review & editing. Roberto Scotti: formal analysis. Cinzia Cristiani: conceptualization, methodology, investigation, writing original draft preparation, Writing—review & editing, supervision. Elisabetta Finocchio: methodology, investigation, writing original draft preparation and Writing—review & editing.

Funding
The authors did not receive support from any organization for the submitted work.

Data availability
Data are available from the authors upon request.

Declarations

Competing interests
The authors have no relevant financial or non-financial interests to disclose.

Author details
[1]Department of Chemistry, Materials and Chemical Engineering "Giulio Natta", Politecnico di Milano, Piazza Leonardo Da Vinci 32, 20133 Milano, Italy. [2]Department of Veterinary Medicine and Animal Sciences—DIVAS, Università degli Studi di Milano, Via Dell'Università 6, 26900 Lodi, Italy. [3]Department of Veterinary Sciences, Università degli Studi di Messina, Viale Giovanni Palatucci 13, 98168 Messina, Italy. [4]Department of Materials Science, INSTM, Università degli Studi di Milano Bicocca, Via R. Cozzi 55, 20125 Milano, Italy. [5]Department of Engineering "Enzo Ferrari", Università degli Studi di Modena E Reggio Emilia (UNIMORE), Via Vivarelli 10/1, 41125 Modena, Italy. [6]Institute for Photonics and Nanotechnologies-CNR, Via alla Cascata 56/C, 38123 Povo, TN, Italy. [7]Department of Civil, Chemical and Environmental Engineering—DICCA, Università di Genova (UniGe), Via All'Opera Pia 15, 16145 Genoa, Italy. [8]Università degli Studi di Modena e Reggio Emilia, Via Università 4, 41121 Modena, Italy.

Received: 8 August 2024 Revised: 25 November 2025 Accepted: 11 December 2025
Published online: 03 February 2026

References

Albernaz-Gonçalves R, Olmos Antillón G, Hötzel MJ (2022) Linking animal welfare and antibiotic use in pig farming—a review. Animals 12:216. https://doi.org/10.3390/ani12020216

Alsawy T, Rashad E, El-Qelish M, Mohammed RH (2022) A comprehensive review on the chemical regeneration of biochar adsorbent for sustainable wastewater treatment. NPJ Clean Water 5:29. https://doi.org/10.1038/s41545-022-00172-3

Ange KD, Eisemann JH, Argenzio RA, Almond GW, Blikslager AT (2000) Effects of feed physical form and buffering solutes on water disappearance and proximal stomach pH in swine. J Anim Sci 78:2344. https://doi.org/10.2527/2000.7892344x

Barth A (2007) Infrared spectroscopy of proteins. Biochim Biophys Acta (BBA) Bioenerg 1767:1073–1101. https://doi.org/10.1016/j.bbabio.2007.06.004

Batista EMCC, Shultz J, Matos TTS, Fornari MR, Ferreira TM, Szpoganicz B, De Freitas RA, Mangrich AS (2018) Effect of surface and porosity of biochar on water holding capacity aiming indirectly at preservation of the Amazon biome. Sci Rep 8:10677. https://doi.org/10.1038/s41598-018-28794-z

Borchard N, Schirrmann M, Cayuela ML, Kammann C, Wrage-Mönnig N, Estavillo JM, Fuertes-Mendizábal T, Sigua G, Spokas K, Ippolito JA, Novak J (2019) Biochar, soil and land-use interactions that reduce nitrate leaching and N2O emissions: a meta-analysis. Sci Total Environ 651:2354–2364. https://doi.org/10.1016/j.scitotenv.2018.10.060

Brewer CE, Chuang VJ, Masiello CA, Gonnermann H, Gao X, Dugan B, Driver LE, Panzacchi P, Zygourakis K, Davies CA (2014) New approaches to measuring biochar density and porosity. Biomass Bioenergy 66:176–185. https://doi.org/10.1016/j.biombioe.2014.03.059

Brown RC (2021) The role of pyrolysis and gasification in a carbon negative economy. Processes 9:882. https://doi.org/10.3390/pr9050882

Caporale AG, Pigna M, Sommella A, Conte P (2014) Effect of pruning-derived biochar on heavy metals removal and water dynamics. Biol Fertil Soils 50:1211–1222. https://doi.org/10.1007/s00374-014-0960-5

Castañeda-Barba S, Top EM, Stalder T (2024) Plasmids, a molecular cornerstone of antimicrobial resistance in the One Health era. Nat Rev Microbiol 22:18–32. https://doi.org/10.1038/s41579-023-00926-x

Cederlund H, Börjesson E, Stenström J (2017) Effects of a wood-based biochar on the leaching of pesticides chlorpyrifos, diuron, glyphosate and MCPA. J Environ Manage 191:28–34. https://doi.org/10.1016/j.jenvman.2017.01.004

Cegielska-Radziejewska R, Leśnierowski G, Kijowski J (2008) Properties and application of egg white lysozyme and its modified preparations—a review. Pol J Food Nutr Sci 58(1):5–10
Cha JS, Park SH, Jung S-C, Ryu C, Jeon J-K, Shin M-C, Park Y-K (2016) Production and utilization of biochar: a review. J Ind Eng Chem 40:1–15. https://doi.org/10.1016/j.jiec.2016.06.002
5220 Chemical Oxygen Demand (COD) (2017) Standard methods for the examination of water and wastewater. American Public Health Association, Washington, DC
Chen W, Meng J, Han X, Lan Y, Zhang W (2019) Past, present, and future of biochar. Biochar 1:75–87. https://doi.org/10.1007/s42773-019-00008-3
Chu GM, Kim JH, Kang SN, Song YM (2013a) Effects of dietary bamboo charcoal on the carcass characteristics and meat quality of fattening pigs. Korean J Food Sci Anim Resour 33:348–355. https://doi.org/10.5851/kosfa.2013.33.3.348
Chu GM, Kim JH, Kim HY, Ha JH, Jung MS, Song Y, Cho JH, Lee SJ, Ibrahim RIH, Lee SS, Song YM (2013b) Effects of bamboo charcoal on the growth performance, blood characteristics and noxious gas emission in fattening pigs. J Appl Anim Res 41:48–55. https://doi.org/10.1080/09712119.2012.738219
Cristiani C, Finocchio E, Rossi L, Giromini C, Dell'Anno M, Panseri S, Bellotto M (2021) Natural clays as potential amino acids carriers for animal nutrition application. Appl Sci 11:5669. https://doi.org/10.3390/app11125669
Cromwell GL (2002) Why and how antibiotics are used in swine production. Anim Biotechnol 13:7–27. https://doi.org/10.1081/ABIO-120005767
De S, Medeiros BG, Souza MP, Pinheiro AC, Bourbon AI, Cerqueira MA, Vicente AA, Carneiro-da-Cunha MG (2014) Physical characterisation of an alginate/lysozyme nano-laminate coating and its evaluation on 'Coalho' cheese shelf life. Food Bioprocess Technol 7:1088–1098. https://doi.org/10.1007/s11947-013-1097-5
Dehkhoda AM, West AH, Ellis N (2010) Biochar based solid acid catalyst for biodiesel production. Appl Catal Gen 382:197–204. https://doi.org/10.1016/j.apcata.2010.04.051
Dell'Anno M, Hejna M, Sotira S, Caprarulo V, Reggi S, Pilu R, Miragoli F, Callegari ML, Panseri S, Rossi L (2020) Evaluation of leonardite as a feed additive on lipid metabolism and growth of weaned piglets. Anim Feed Sci Technol 266:114519. https://doi.org/10.1016/j.anifeedsci.2020.114519
Dell'Anno M, Scaglia E, Reggi S, Grossi S, Sgoifo Rossi CA, Frazzini S, Caprarulo V, Rossi L (2023) Evaluation of tributyrin supplementation in milk replacer on diarrhoea occurrence in preweaning Holstein calves. Anim 17:100791. https://doi.org/10.1016/j.animal.2023.100791
Dragoni I, Balzaretti C, Rossini S, Rossi L, Dell'Orto V, Baldi A (2011) Detection of hen lysozyme on proteic profiles of Grana Padano cheese through SELDI-TOF MS high-throughput technology during the ripening process. Food Anal Methods 4:233–239. https://doi.org/10.1007/s12161-010-9146-4
Elkordy AA, Forbes RT, Barry BW (2002) Integrity of crystalline lysozyme exceeds that of a spray-dried form. Int J Pharm 247:79–90. https://doi.org/10.1016/S0378-5173(02)00379-4
Ferraboschi P, Ciceri S, Grisenti P (2021) Applications of lysozyme, an innate immune defense factor, as an alternative antibiotic. Antibiotics 10:1534. https://doi.org/10.3390/antibiotics10121534
Gerlach A (2014) Oral application of charcoal and humic acids to dairy cows influences clostridium botulinum blood serum antibody level and glyphosate excretion in urine. J Clin Toxicol. https://doi.org/10.4172/2161-0495.1000186
González ME, Cea M, Sangaletti N, González A, Toro C, Diez MC, Moreno N, Querol X, Navia R (2013) Biochar derived from agricultural and forestry residual biomass: characterization and potential application for enzymes immobilization. J Biobased Mater Bioenergy 7:724–732. https://doi.org/10.1166/jbmb.2013.1373
Guagliano M, Cristiani C, Dell'Anno M, Dotelli G, Finocchio E, Lacalamita M, Mesto E, Reggi S, Rossi L, Schingaro E (2023a) A commercial clay-based material as a carrier for targeted lysozyme delivery in animal feed. Nanomaterials 13:2965. https://doi.org/10.3390/nano13222965
Guagliano M, Dell'Anno M, Dotelli G, Finocchio E, Lacalamita M, Mesto E, Reggi S, Rossi L, Schingaro E, Staltari E, Cristiani C (2023b) Lysozyme-mineral clay systems: comparison of interaction for controlled release in feed application. Minerals 13:660. https://doi.org/10.3390/min13050660
Guo X, Liu H, Zhang J (2020) The role of biochar in organic waste composting and soil improvement: a review. Waste Manag 102:884–899. https://doi.org/10.1016/j.wasman.2019.12.003
Henze LJ, Koehl NJ, Bennett-Lenane H, Holm R, Grimm M, Schneider F, Weitschies W, Koziolek M, Griffin BT (2021) Characterization of gastrointestinal transit and luminal conditions in pigs using a telemetric motility capsule. Eur J Pharm Sci 156:105627. https://doi.org/10.1016/j.ejps.2020.105627
Hong M, Zhang L, Tan Z, Huang Q (2019) Effect mechanism of biochar's zeta potential on farmland soil's cadmium immobilization. Environ Sci Pollut Res 26:19738–19748. https://doi.org/10.1007/s11356-019-05298-5
Hu YJ, Cowling BJ (2020) Reducing antibiotic use in livestock, China. Bull World Health Organ 98:360–361. https://doi.org/10.2471/BLT.19.243501
Ibrahim H, Aoki T, Pellegrini A (2002) Strategies for new antimicrobial proteins and peptides: lysozyme and aprotinin as model molecules. Curr Pharm des 8:671–693. https://doi.org/10.2174/1381612023395349
Jaiswal AK, Frenkel O, Tsechansky L, Elad Y, Graber ER (2018) Immobilization and deactivation of pathogenic enzymes and toxic metabolites by biochar: a possible mechanism involved in soilborne disease suppression. Soil Biol Biochem 121:59–66. https://doi.org/10.1016/j.soilbio.2018.03.001
Jeffery S, Verheijen FGA, Van Der Velde M, Bastos AC (2011) A quantitative review of the effects of biochar application to soils on crop productivity using meta-analysis. Agric Ecosyst Environ 144:175–187. https://doi.org/10.1016/j.agee.2011.08.015
Jones S, Bardos RP, Kidd PS, Mench M, De Leij F, Hutchings T, Cundy A, Joyce C, Soja G, Friesl-Hanl W, Herzig R, Menger P (2016) Biochar and compost amendments enhance copper immobilisation and support plant growth in contaminated soils. J Environ Manage 171:101–112. https://doi.org/10.1016/j.jenvman.2016.01.024
Kalus K, Koziel J, Opaliński S (2019) A review of biochar properties and their utilization in crop agriculture and livestock production. Appl Sci 9:3494. https://doi.org/10.3390/app9173494
Kammann C, Ippolito J, Hagemann N, Borchard N, Cayuela ML, Estavillo JM, Fuertes-Mendizabal T, Jeffery S, Kern J, Novak J, Rasse D, Saarnio S, Schmidt H-P, Spokas K, Wrage-Mönnig N (2017) Biochar as a tool to reduce the agricultural greenhouse-gas burden—knowns, unknowns and future research needs. J Environ Eng Landsc Manag 25:114–139. https://doi.org/10.3846/16486897.2017.1319375
Kan T, Strezov V, Evans TJ (2016) Lignocellulosic biomass pyrolysis: a review of product properties and effects of pyrolysis parameters. Renew Sustain Energy Rev 57:1126–1140. https://doi.org/10.1016/j.rser.2015.12.185
Kasapidou E, Sossidou E, Mitlianga P (2015) Fruit and vegetable co-products as functional feed ingredients in farm animal nutrition for improved product quality. Agriculture 5:1020–1034. https://doi.org/10.3390/agriculture5041020
Kim Y-C, Myerson AS (1994) Diffusivity of lysozyme in undersaturated, saturated and supersaturated solutions. J Cryst Growth 143:79–85. https://doi.org/10.1016/0022-0248(94)90370-0
Klank, D.; Goverde, T.; Blum, C. Particle World; technical papers of quantachrome; quantachrome: Klundert, The Netherlands, 2009. www.quantachrome.com. Accessed 17 Mar 2023
Kocherbitov V, Latynis J, Misiūnas A, Barauskas J, Niaura G (2013) Hydration of lysozyme studied by Raman spectroscopy. J Phys Chem B 117:4981–4992. https://doi.org/10.1021/jp4017954
Kummer N, Huguenin-Elie L, Zeller A, Chandorkar Y, Schoeller J, Zuber F, Ren Q, Sinha A, De France K, Fischer P, Campioni S, Nyström G (2023) 2D foam film coating of antimicrobial lysozyme amyloid fibrils onto cellulose nanopapers. Nanoscale Adv 5:5276–5285. https://doi.org/10.1039/D3NA00370A
Leistikow KR, Beattie RE, Hristova KR (2022) Probiotics beyond the farm: benefits, costs, and considerations of using antibiotic alternatives in livestock. Front Antibiot 1:1003912. https://doi.org/10.3389/frabi.2022.1003912
Leng L, Xiong Q, Yang L, Li H, Zhou Y, Zhang W, Jiang S, Li H, Huang H (2021) An overview on engineering the surface area and porosity of biochar. Sci Total Environ 763:144204. https://doi.org/10.1016/j.scitotenv.2020.144204
Li L, Yao Z, You S, Wang C-H, Chong C, Wang X (2019) Optimal design of negative emission hybrid renewable energy systems with biochar production. Appl Energy 243:233–249. https://doi.org/10.1016/j.apenergy.2019.03.183
Liu Y, Zhao X, Li J, Ma D, Han R (2012) Characterization of bio-char from pyrolysis of wheat straw and its evaluation on methylene blue adsorption. Desalination Water Treat 46:115–123. https://doi.org/10.1080/19443994.2012.677408

Liu Q, Zhang Y, Liu B, Amonette JE, Lin Z, Liu G, Ambus P, Xie Z (2018a) How does biochar influence soil N cycle? A meta-analysis. Plant Soil 426:211–225. https://doi.org/10.1007/s11104-018-3619-4
Liu Y, Espinosa CD, Abelilla JJ, Casas GA, Lagos LV, Lee SA, Kwon WB, Mathai JK, Navarro DMDL, Jaworski NW, Stein HH (2018b) Non-antibiotic feed additives in diets for pigs: a review. Anim Nutr 4:113–125. https://doi.org/10.1016/j.aninu.2018.01.007
Lunney JK, Van Goor A, Walker KE, Hailstock T, Franklin J, Dai C (2021) Importance of the pig as a human biomedical model. Sci Transl Med 13:eabd5758. https://doi.org/10.1126/scitranslmed.abd5758
Ma X, Zhou B, Budai A, Jeng A, Hao X, Wei D, Zhang Y, Rasse D (2016) Study of biochar properties by scanning electron microscope – energy dispersive X-ray spectroscopy (SEM-EDX). Commun Soil Sci Plant Anal 47:593–601. https://doi.org/10.1080/00103624.2016.1146742
Mahfuz S, Shang Q, Piao X (2021) Phenolic compounds as natural feed additives in poultry and swine diets: a review. J Anim Sci Biotechnol 12:48. https://doi.org/10.1186/s40104-021-00565-3
Mandal A, Singh N, Purakayastha TJ (2017) Characterization of pesticide sorption behaviour of slow pyrolysis biochars as low cost adsorbent for atrazine and imidacloprid removal. Sci Total Environ 577:376–385. https://doi.org/10.1016/j.scitotenv.2016.10.204
Masschalck B, Van Houdt R, Van Haver EGR, Michiels CW (2001) Inactivation of Gram-Negative Bacteria by lysozyme, denatured lysozyme, and lysozyme-derived peptides under high hydrostatic pressure. Appl Environ Microbiol 67:339–344. https://doi.org/10.1128/AEM.67.1.339-344.2001
Mößeler A, Köttendorf S, Große Liesner V, Kamphues J (2010) Impact of diets' physical form (particle size; meal/pelleted) on the stomach content (dry matter content, pH, chloride concentration) of pigs. Livest Sci 134:146–148. https://doi.org/10.1016/j.livsci.2010.06.121
Noritomi H (2019) Application of biochar to enzyme carrier for stress tolerance of enzymes. In: Abrol V, Sharma P (eds) Biochar—an imperative amendment for soil and the environment. IntechOpen, London
Nunes LJR, Rodrigues AM, Matias JCO, Ferraz AI, Rodrigues AC (2021) Production of biochar from vine pruning: waste recovery in the wine industry. Agriculture 11:489. https://doi.org/10.3390/agriculture11060489
O'Dell JW (1996) The determination of chemical oxygen demand by semi-automated colorimetry. Methods for the determination of metals in environmental samples. Elsevier, Amsterdam, pp 509–521
Oliver WT, Wells JE (2015) Lysozyme as an alternative to growth promoting antibiotics in swine production. J Anim Sci Biotechnol 6:35. https://doi.org/10.1186/s40104-015-0034-z
Oliver WT, Wells JE, Maxwell CV (2014) Lysozyme as an alternative to antibiotics improves performance in nursery pigs during an indirect immune challenge1,2. J Anim Sci 92:4927–4934. https://doi.org/10.2527/jas.2014-8033
Ortiz Sanjuán JM, Manzanilla EG, Cabrera-Rubio R, Crispie F, Cotter PD, Garrido JJ, Ekhlas D, O'Neill L, Argüello H (2024) Fine-tuning of post-weaning pig microbiome structure and functionality by in-feed zinc oxide and antibiotics use. Front Cell Infect Microbiol 14:1354449. https://doi.org/10.3389/fcimb.2024.1354449
Pallarés J, González-Cencerrado A, Arauzo I (2018) Production and characterization of activated carbon from barley straw by physical activation with carbon dioxide and steam. Biomass Bioenergy 115:64–73. https://doi.org/10.1016/j.biombioe.2018.04.015
Pandey D, Daverey A, Dutta K, Arunachalam K (2022) Bioremoval of toxic malachite green from water through simultaneous decolorization and degradation using laccase immobilized biochar. Chemosphere 297:134126. https://doi.org/10.1016/j.chemosphere.2022.134126
Pawar VK, Meher JG, Singh Y, Chaurasia M, Surendar Reddy B, Chourasia MK (2014) Targeting of gastrointestinal tract for amended delivery of protein/peptide therapeutics: strategies and industrial perspectives. J Controlled Release 196:168–183. https://doi.org/10.1016/j.jconrel.2014.09.031
Picchi G, Silvestri S, Cristoforetti A (2013) Vineyard residues as a fuel for domestic boilers in Trento Province (Italy): comparison to wood chips and means of polluting emissions control. Fuel 113:43–49. https://doi.org/10.1016/j.fuel.2013.05.058
Prestinaci F, Pezzotti P, Pantosti A (2015) Antimicrobial resistance: a global multifaceted phenomenon. Pathog Glob Health 109:309–318. https://doi.org/10.1179/2047773215Y.0000000030
Ramirez BC, Xin H, Halbur PG, Beermann DH, Hansen SL, Linhares DCL, Peschel JM, Rademacher CJ, Reecy JM, Ross JW, Shepherd TA, Koltes JE (2019) At the intersection of industry, academia, and government: how do we facilitate productive precision livestock farming in practice? Animals 9:635. https://doi.org/10.3390/ani9090635
Reggi S, Frazzini S, Torresani MC, Guagliano M, Cristiani C, Pilu SR, Ghidoli M, Rossi L (2024) Metabolomic profiling and functional characterization of biochar from vine pruning residues for applications in animal feed. Animals 14:3440. https://doi.org/10.3390/ani14233440
Reggi S, Frazzini S, Pedrazzi S, Ghidoli M, Torresani MC, Puglia M, Morselli N, Guagliano M, Cristiani C, Pilu SR, Onelli E, Moscatelli A, Rossi L (2025) Metabolomic insights into the potential of chestnut biochar as a functional feed ingredient. Appl Sci 15:1084. https://doi.org/10.3390/app15031084
Robinson TP, Bu DP, Carrique-Mas J, Fèvre EM, Gilbert M, Grace D, Hay SI, Jiwakanon J, Kakkar M, Kariuki S, Laxminarayan R, Lubroth J, Magnusson U, Thi Ngoc P, Van Boeckel TP, Woolhouse MEJ (2017) Antibiotic resistance: mitigation opportunities in livestock sector development. Animal 11:1–3. https://doi.org/10.1017/S1751731116001828
Rossi L, Dell'Anno M, Turin L, Reggi S, Lombardi A, Alborali GL, Filipe J, Riva F, Riccaboni P, Scanziani E, Dall'Ara P, Demartini E, Baldi A (2023) Tobacco seed-based oral vaccination against Verocytotoxic O138 *Escherichia coli* as alternative approach to antibiotics in weaned piglets. Antibiotics 12:715. https://doi.org/10.3390/antibiotics12040715
Ruiz B, Ferrera-Lorenzo N, Fuente E (2017) Valorisation of lignocellulosic wastes from the candied chestnut industry. Sustainable activated carbons for environmental applications. J Environ Chem Eng 5:1504–1515. https://doi.org/10.1016/j.jece.2017.02.028
Safaei Khorram M, Zhang Q, Lin D, Zheng Y, Fang H, Yu Y (2016) Biochar: a review of its impact on pesticide behavior in soil environments and its potential applications. J Environ Sci 44:269–279. https://doi.org/10.1016/j.jes.2015.12.027
Sakhiya AK, Anand A, Kaushal P (2020) Production, activation, and applications of biochar in recent times. Biochar 2:253–285. https://doi.org/10.1007/s42773-020-00047-1
Schmidt H-P, Hagemann N, Draper K, Kammann C (2019) The use of biochar in animal feeding. PeerJ 7:e7373. https://doi.org/10.7717/peerj.7373
Sha Z, Li Q, Lv T, Misselbrook T, Liu X (2019) Response of ammonia volatilization to biochar addition: a meta-analysis. Sci Total Environ 655:1387–1396. https://doi.org/10.1016/j.scitotenv.2018.11.316
Silvetti T, Morandi S, Hintersteiner M, Brasca M (2017) Use of hen egg white lysozyme in the food industry. In: Silvetti T, Morandi S, Hintersteiner M, Brasca M (eds) Egg innovations and strategies for improvements. Academic Press, Cambridge, pp 233–242
Squillaci G, Apone F, Michele Sena L, Carola A, Tito A, Bimonte M, De Lucia A, Colucci G, La Cara F, Morana A (2018) Chestnut (*Castanea sativa* Mill.) industrial wastes as a valued bioresource for the production of active ingredients. Process Biochem 64:228-236. https://doi.org/10.1016/j.procbio.2017.09.017. https://www.sciencedirect.com/science/article/pii/S1359511317310073
Waters CL, Janupala RR, Mallinson RG, Lobban LL (2017) Staged thermal fractionation for segregation of lignin and cellulose pyrolysis products: an experimental study of residence time and temperature effects. J Anal Appl Pyrolysis 126:380–389. https://doi.org/10.1016/j.jaap.2017.05.008
WHO Regional Office for Europe and European Centre for Disease Prevention and Control (2025). Surveillance of antimicrobial resistance in Europe, 2024 data: executive summary. Copenhagen: WHO Regional Office for Europe
World Health Organization. (2019). Monitoring and evaluation of the global action plan on antimicrobial resistance: framework and recommended indicators.
Wu T, Jiang Q, Wu D, Hu Y, Chen S, Ding T, Ye X, Liu D, Chen J (2019) What is new in lysozyme research and its application in food industry? A review. Food Chem 274:698–709. https://doi.org/10.1016/j.foodchem.2018.09.017
www.mur.gov.it
www.research-and-innovation.ec.europa.eu
Yan Y, Manickam S, Lester E, Wu T, Pang CH (2021) Synthesis of graphene oxide and graphene quantum dots from miscanthus via ultrasound-assisted mechano-chemical cracking method. Ultrason Sonochem 73:105519. https://doi.org/10.1016/j.ultsonch.2021.105519
Yang H, Yan R, Chen H, Lee DH, Zheng C (2007) Characteristics of hemicellulose, cellulose and lignin pyrolysis. Fuel 86:1781–1788. https://doi.org/10.1016/j.fuel.2006.12.013

Yi Q, Qi F, Cheng G, Zhang Y, Xiao B, Hu Z, Liu S, Cai H, Xu S (2013) Thermogravimetric analysis of co-combustion of biomass and biochar. J Therm Anal Calorim 112:1475–1479. https://doi.org/10.1007/s10973-012-2744-1

Yu S, Wang L, Li Q, Zhang Y, Zhou H (2022) Sustainable carbon materials from the pyrolysis of lignocellulosic biomass. Mater Today Sustain 19:100209. https://doi.org/10.1016/j.mtsust.2022.100209

Yuan J-H, Xu R-K, Zhang H (2011) The forms of alkalis in the biochar produced from crop residues at different temperatures. Bioresour Technol 102:3488–3497. https://doi.org/10.1016/j.biortech.2010.11.018

Zambon I, Colantoni A, Cecchini M, Mosconi E (2018) Rethinking sustainability within the Viticulture Realities Integrating Economy, Landscape and Energy. Sustainability 10:320. https://doi.org/10.3390/su10020320

Zhang X, Wang H, He L, Lu K, Sarmah A, Li J, Bolan NS, Pei J, Huang H (2013) Using biochar for remediation of soils contaminated with heavy metals and organic pollutants. Environ Sci Pollut Res 20:8472–8483. https://doi.org/10.1007/s11356-013-1659-0

Zhang B, Tao H, Niu X, Li S, Chen H-Q (2017) Lysozyme distribution, structural identification, and in vitro release of starch-based microgel-lysozyme complexes. Food Chem 227:137–141. https://doi.org/10.1016/j.foodchem.2017.01.073

Zhou P, Adeel M, Guo M, Ge L, Shakoor N, Li M, Li Y, Wang G, Rui Y (2022) Characterisation of biochar produced from two types of chestnut shells for use in remediation of cadmium- and lead-contaminated soil. Crop Pasture Sci 74:147–156. https://doi.org/10.1071/CP21297

Zou L, Xiong X, Liu H, Zhou J, Liu Y, Yin Y (2019) Effects of dietary lysozyme levels on growth performance, intestinal morphology, immunity response and microbiota community of growing pigs: dietary lysozyme levels in growing pigs. J Sci Food Agric 99:1643–1650. https://doi.org/10.1002/jsfa.9348